

# Transverse-momentum resummation: a perturbative study of $Z$ production at the Tevatron

Giuseppe Bozzi<sup>(a)</sup>, Stefano Catani<sup>(b)</sup>,  
Giancarlo Ferrera<sup>(b)</sup>, Daniel de Florian<sup>(c)</sup> and Massimiliano Grazzini<sup>(b)</sup>

<sup>(a)</sup>Institut für Theoretische Physik, Universität Karlsruhe  
P.O.Box 6980, D-76128 Karlsruhe, Germany

<sup>(b)</sup>INFN, Sezione di Firenze and Dipartimento di Fisica, Università di Firenze,  
I-50019 Sesto Fiorentino, Florence, Italy

<sup>(c)</sup>Departamento de Física, FCEYN, Universidad de Buenos Aires,  
(1428) Pabellón 1 Ciudad Universitaria, Capital Federal, Argentina

## Abstract

We consider transverse-momentum ( $q_T$ ) resummation for Drell–Yan lepton pair production in hadron collisions. At small values of  $q_T$ , the logarithmically-enhanced QCD contributions are resummed up to next-to-leading logarithmic accuracy. At intermediate and large values of  $q_T$ , resummation is consistently combined with the fixed-order perturbative result. We present numerical results for  $e^+e^-$  pairs from the decay of  $Z$  bosons produced at Tevatron energies. We perform a detailed study of the scale dependence of the results to estimate the corresponding perturbative uncertainty. We comment on the comparison with the available Tevatron data.

# 1 Introduction

The production of  $W$  and  $Z$  bosons in hadron collisions is important for physics studies within and beyond the Standard Model (SM). The large production rates and clean experimental signatures make these processes standard candles for calibration purposes. At the LHC,  $W$  and  $Z$  boson production has even been proposed as a luminosity monitor. In the search for new physics, an excess of di-lepton events with large invariant mass or missing energy may signal the production of new gauge bosons or of SUSY particles.

Because of the above reasons, it is essential to have accurate theoretical predictions for the vector-boson production cross sections and distributions. Theoretical predictions with high precision demand detailed computations of radiative corrections. The QCD corrections to the total cross section [1] and to the rapidity distribution of the vector boson [2] are known up to the next-to-next-to-leading order (NNLO) in the strong coupling  $\alpha_S$ . The fully exclusive NNLO calculation, including the leptonic decay of the vector boson, has been completed more recently [3]. As for electroweak effects, full  $\mathcal{O}(\alpha)$  corrections have been computed for both  $W$  [4] and  $Z$  production [5].

Among the various distributions, an important role is played by the transverse-momentum ( $q_T$ ) spectrum of the vector boson. In the case of  $W$  production, the uncertainty in the shape of the  $q_T$  spectrum directly affects the measurement of the  $W$  mass. A good understanding of the  $q_T$  spectrum of the  $Z$  boson gives important information on the production mechanism of the  $W$  boson.

In the region where  $q_T \sim m_V$ ,  $m_V$  being the mass of the vector boson, the QCD perturbative series is controlled by a small expansion parameter,  $\alpha_S(m_V)$ , and fixed-order calculations are theoretically justified. In this region, the QCD radiative corrections are known up to next-to-leading order (NLO) [6, 7, 8]. In the small  $q_T$  region ( $q_T \ll m_V$ ), the convergence of the fixed-order expansion is spoiled, since the coefficients of the perturbative series are enhanced by powers of large logarithmic terms,  $\alpha_S^n \ln^m(m_V^2/q_T^2)$ . To obtain reliable predictions, these terms have to be resummed to all perturbative orders.

The method to systematically perform all-order resummation of classes of logarithmically-enhanced terms at small  $q_T$  is known [9]–[17]. The resummed and fixed-order procedures at small and large values of  $q_T$  can then be matched at intermediate values of  $q_T$ , to obtain QCD predictions for the entire range of transverse momenta. Phenomenological studies of the vector-boson  $q_T$  distribution have been performed by combining resummed and fixed-order perturbation theory at various levels of accuracy [18]–[28].

In Refs. [17, 29] we have proposed a method to perform transverse-momentum resummation that introduces some novel features. The resummed distribution is factorized in terms of a universal transverse-momentum form factor and a single process-dependent hard function. In the small- $q_T$  region, the logarithmic terms of the form factor are systematically resummed in exponential form by working in impact-parameter and Mellin-moment space. A constraint of perturbative unitarity is imposed on the resummed terms, to the purpose of reducing the effect of unjustified higher-order contributions at large values of  $q_T$  and, especially, at intermediate values of  $q_T$ . This constraint decreases the uncertainty in the matching procedure of the resummed and fixed-order contributions. The method has so far been applied to SM Higgs boson production [30, 29, 31],  $WW$  [32] and  $ZZ$  [33] production, and slepton pair production [34]. Related methods on transverse-

momentum resummation have been applied to the transversely-polarized Drell–Yan (DY) process [35] and longitudinally-polarized semi-inclusive deep-inelastic scattering (SIDIS) [36].

The explicit form of the universal form factor is known up to next-to-leading logarithmic (NLL) [14, 37] and next-to-next-to-leading logarithmic (NNLL) [38, 39, 40] level. The general form of the process dependent hard function is known up to the first relative order in  $\alpha_S$  [40]. The hard function has been computed up to the second relative order in  $\alpha_S$  only in the case of SM Higgs boson production [41].

In the present paper we concentrate on DY lepton pair production, and we apply the resummation formalism of Ref. [29] to the production of  $Z$  bosons at Tevatron energies. In this work, we limit ourselves to presenting results up to NLL accuracy. We perform a detailed study of the scale dependence of our results and we provide an estimate of the corresponding perturbative uncertainty. We also comment on the comparison with the available Tevatron data. In this way, we set the stage for a forthcoming NNLL analysis, which will be possible once the computation of the hard function up to second order is completed.

The paper is organized as follows. In Sect. 2 we briefly review our resummation formalism and we comment on its application to vector boson production in hadron collisions. In Sect. 3 we present numerical results on  $Z$  boson production at the Tevatron. The fixed-order and resummed predictions are discussed and compared with the data in Sect. 3.1 and Sect. 3.2, respectively. Our results are summarized in Sect. 4.

## 2 Transverse-momentum resummation

The resummation formalism that we use in this paper is discussed in detail in Ref. [29]. The formalism can be applied to a generic process in which a high-mass system of non strongly-interacting particles is produced in hadron–hadron collisions. In this section we briefly recall the main points of the formalism, by considering the specific case of the production of a vector boson  $V$  ( $V = W^+, W^-, Z/\gamma^*$ ) that subsequently decays in a lepton pair of invariant mass  $M$ .

The transverse-momentum differential cross section for this process is written as

$$\frac{d\sigma_V}{dq_T^2}(q_T, M, s) = \sum_{a,b} \int_0^1 dx_1 \int_0^1 dx_2 f_{a/h_1}(x_1, \mu_F^2) f_{b/h_2}(x_2, \mu_F^2) \frac{d\hat{\sigma}_{Vab}}{dq_T^2}(q_T, M, \hat{s}; \alpha_S(\mu_R^2), \mu_R^2, \mu_F^2) , \quad (1)$$

where  $f_{a/h}(x, \mu_F^2)$  ( $a = q, \bar{q}, g$ ) are the parton densities of the colliding hadrons ( $h_1$  and  $h_2$ ) at the factorization scale  $\mu_F$ ,  $d\hat{\sigma}_{Vab}/dq_T^2$  are the partonic cross sections,  $s$  ( $\hat{s} = x_1 x_2 s$ ) is the hadronic (partonic) centre-of-mass energy, and  $\mu_R$  is the renormalization scale.

The resummation is performed at the level of the partonic cross section, which is first decomposed as follows:

$$\frac{d\hat{\sigma}_{Vab}}{dq_T^2} = \frac{d\hat{\sigma}_{Vab}^{(\text{res.})}}{dq_T^2} + \frac{d\hat{\sigma}_{Vab}^{(\text{fin.})}}{dq_T^2} . \quad (2)$$

The ‘resummed’ component,  $d\hat{\sigma}_{Vab}^{(\text{res.})}$ , of the cross section contains all the logarithmically-enhanced contributions at small  $q_T$ , and it has to be evaluated by resumming them to all orders in  $\alpha_S$ . The

‘finite’ component,  $d\hat{\sigma}_{Vab}^{(\text{fin.})}$ , is free of such contributions, and it can thus be evaluated at fixed order in perturbation theory.

The resummation procedure of the logarithmic terms is carried out in the impact-parameter space. The resummed component of the partonic cross section is then obtained by performing the inverse Fourier (Bessel) transformation with respect to the impact parameter  $b$ . We write:

$$\frac{d\hat{\sigma}_{Vab}^{(\text{res.})}}{dq_T^2}(q_T, M, \hat{s}; \alpha_S(\mu_R^2), \mu_R^2, \mu_F^2) = \frac{M^2}{\hat{s}} \int_0^\infty db \frac{b}{2} J_0(bq_T) \mathcal{W}_{ab}^V(b, M, \hat{s}; \alpha_S(\mu_R^2), \mu_R^2, \mu_F^2), \quad (3)$$

where  $J_0(x)$  is the 0th-order Bessel function. The factor  $\mathcal{W}$  embodies the all-order dependence on the large logarithms  $\ln(M^2b^2)$  at large  $b$ , which correspond to the  $q_T$ -space terms  $\ln(M^2/q_T^2)$  at small  $q_T$ . By considering the  $N$ -moments  $\mathcal{W}_N$  of  $\mathcal{W}$  with respect to the variable  $z = M^2/\hat{s}$  at fixed  $M$ , the resummation structure of  $\mathcal{W}_{ab,N}^V$  can be factorized and organized in exponential form<sup>†</sup>:

$$\begin{aligned} \mathcal{W}_N^V(b, M; \alpha_S(\mu_R^2), \mu_R^2, \mu_F^2) &= \mathcal{H}_N^V(M, \alpha_S(\mu_R^2); M^2/\mu_R^2, M^2/\mu_F^2, M^2/Q^2) \\ &\times \exp\{\mathcal{G}_N(\alpha_S(\mu_R^2), L; M^2/\mu_R^2, M^2/Q^2)\}, \end{aligned} \quad (4)$$

where we have defined the logarithmic expansion parameter  $L$ ,

$$L \equiv \ln \frac{Q^2 b^2}{b_0^2}, \quad (5)$$

and the coefficient  $b_0 = 2e^{-\gamma_E}$  ( $\gamma_E = 0.5772\dots$  is the Euler number) has a kinematical origin. The function  $\mathcal{H}_N^V$  does not depend on the impact parameter  $b$ , and it includes all the perturbative terms that behave as constants in the limit  $b \rightarrow \infty$ . The function  $\mathcal{G}_N$  includes the complete dependence on  $b$  and, in particular, it contains all the terms that order-by-order in  $\alpha_S$  are logarithmically divergent as  $b \rightarrow \infty$ .

This separation (actually, factorization) between finite and divergent (or logarithmically-enhanced) terms involves some degree of arbitrariness. The arbitrariness is parametrized by the introduction of the resummation scale  $Q$  [29], which sets the scale of the expansion parameter  $L$  in Eq. (5). Although the resummation factor  $\mathcal{W}_N^V$  does not depend on  $Q$  when evaluated at each fixed order in  $\alpha_S$ , its explicit dependence on  $Q$  appears when  $\mathcal{W}_N^V$  (and, more precisely,  $\mathcal{G}_N$ ) is computed by truncation of the resummed expression at some level of logarithmic accuracy (see Eq. (6) below). The resummation scale  $Q$  has to be chosen of the order of the hard scale  $M$ ; variations of  $Q$  around  $M$  can then be used to estimate the effect of yet uncalculated higher-order logarithmic contributions.

All the large logarithmic terms  $\alpha_S^n L^m$ , with  $1 \leq m \leq 2n$ , are included in the form factor  $\exp\{\mathcal{G}_N\}$  on the right-hand side of Eq. (4). More precisely, all the logarithmic contributions to  $\mathcal{G}_N$  with  $n+2 \leq m \leq 2n$  are vanishing. Therefore, the exponent  $\mathcal{G}_N$  can be organized in classes of logarithmic contributions that can systematically be expanded in powers of  $\alpha_S = \alpha_S(\mu_R^2)$ , at fixed value of  $\lambda = \alpha_S L$ . The logarithmic expansion of  $\mathcal{G}_N$  reads

$$\begin{aligned} \mathcal{G}_N(\alpha_S, L; M^2/\mu_R^2, M^2/Q^2) &= L g^{(1)}(\alpha_S L) + g_N^{(2)}(\alpha_S L; M^2/\mu_R^2, M^2/Q^2) \\ &+ \frac{\alpha_S}{\pi} g_N^{(3)}(\alpha_S L, M^2/\mu_R^2, M^2/Q^2) + \dots \end{aligned} \quad (6)$$

---

<sup>†</sup>Here, to simplify the notation, flavour indices are understood. In other words, we limit ourselves to discussing the flavour non-singlet contribution. A complete discussion of the exponentiation structure in the general case can be found in Appendix A of Ref. [29].

where the term  $L g^{(1)}$  collects the leading logarithmic (LL) contributions, the function  $g_N^{(2)}$  includes the NLL contributions,  $g_N^{(3)}$  controls the NNLL terms and so forth.

An important feature of the resummation formalism [29] is that the form factor  $\exp\{\mathcal{G}_N\}$  is process independent (and independent of the factorization scale, as well). In other words, the functions  $g_N^{(i)}$  are universal: they only depend on the flavour of the partons that contribute to the cross section in each specific partonic channel. More precisely, each function  $g_N^{(i)}$  has a known functional form that is completely specified [12, 16] in terms of few perturbatively-computable (and process independent) coefficients and of the customary parton anomalous dimensions  $\gamma_{ab,N}(\alpha_S)$ . These perturbative coefficients, which are flavour-dependent, are usually denoted by  $A_a^{(n)}$ ,  $B_a^{(n)}$  and  $C_{ab,N}^{(n)}$ . The explicit expressions of  $g_N^{(i)}$  up to  $i = 3$  can be found in Ref. [29]. In the case of DY production (and in any production process that occurs through  $q\bar{q}$  annihilation at the Born level), the LL function  $g^{(1)}$  depends on the coefficient  $A_q^{(1)} = C_F$ , the NLL function  $g_N^{(2)}$  also depends on  $B_q^{(1)}$  and  $A_q^{(2)}$  [14], and the NNLL function  $g_N^{(3)}$  also depends on  $C_{qa,N}^{(1)}$  ( $a = q, g$ ) [38],  $B_q^{(2)}$  [39, 40] and  $A_q^{(3)}$ . All these coefficients are known, with the sole exception of  $A_q^{(3)}$ . It is usually assumed that the value of  $A_q^{(3)}$  is the same as the one [42, 43] that appears in resummed calculations of soft-gluon contributions near partonic threshold.

To compute the resummed component of the partonic cross section, Eq. (4) has to be inserted in the right-hand side of Eq. (3). Using the expression in Eq. (6), the resummation of the large logarithmic contributions in  $\exp\{\mathcal{G}_N\}$  affects not only the small- $q_T$  region ( $q_T \ll M$ ), but also the large- $q_T$  region ( $q_T \sim M$ ). This can easily be understood by observing that the logarithmic expansion parameter  $L$  is divergent when  $b \rightarrow 0$ . To avoid the introduction of large and unjustified higher-order contributions in the small- $b$  (or, equivalently, large- $q_T$ ) region, the logarithmic variable  $L$  in Eq. (5) is replaced by the variable  $\tilde{L}$  [29]:

$$L \rightarrow \tilde{L} \quad , \quad \tilde{L} \equiv \ln \left( \frac{Q^2 b^2}{b_0^2} + 1 \right) . \quad (7)$$

The variables  $L$  and  $\tilde{L}$  are equivalent (to arbitrary logarithmic accuracy) when  $Qb \gg 1$ , but they lead to a different behaviour of the form factor at small values of  $b$  (i.e. large values of  $q_T$ ). In fact, when  $Qb \ll 1$  we have  $\tilde{L} \rightarrow 0$  and  $\exp\{\mathcal{G}_N\} \rightarrow 1$ . The replacement<sup>‡</sup> in Eq. (7) has thus a twofold consequence [29]: it reduces the impact of resummation at large values of  $q_T$ , and it acts as a constraint of perturbative unitarity since it allows us to exactly recover the fixed-order value of the total cross section upon integration over  $q_T$  of the resummed calculation of  $d\sigma/dq_T$ . (i.e., the resummed terms give a vanishing contribution to the total cross section).

The process dependence (as well as the factorization scale dependence) of the resummation factor  $\mathcal{W}_N^V$  is fully encoded in the hard function  $\mathcal{H}_N^V$  on the right-hand side of Eq. (4). Since this

---

<sup>‡</sup>We observe that the divergent behaviour of the logarithmic parameter  $\ln(M^2 b^2)$  when  $b \rightarrow 0$  can be removed by a generic replacement of type  $\ln(M^2 b^2) \rightarrow L_c = \ln(M^2 b^2 + c)$ , where  $c$  is some positive constant of order unity. The effect of the constant  $c$  can be rewritten as  $L_c = \tilde{L}_c + \ln c$ , where  $\tilde{L}_c = \ln(M^2 b^2/c + 1)$ . Using the variable  $L_c$  as argument of the form factor  $\exp\{\mathcal{G}_N\}$  would spoil the constraint of perturbative unitarity, since the term  $\ln c$  in  $L_c$  does not vanish at  $b = 0$ . We are interested to maintain this constraint and, therefore, we have to remove the term  $\ln c$  from  $L_c$  and we are left with the variable  $\tilde{L}_c$ . We note that  $\tilde{L}_c$  is completely analogous to the logarithmic variable  $\tilde{L}$  in Eq. (7) (e.g., we can simply set  $c = b_0^2 M^2 / Q^2$ ). In particular, the quantitative effect of choosing different values of the constant  $c$  in  $\tilde{L}_c$  is completely equivalent to the effect of using different values of the resummation scale  $Q$  in  $\tilde{L}$ .

function does not contain large logarithmic terms to be resummed, it can be expanded in powers of  $\alpha_S = \alpha_S(\mu_R^2)$  as follows:

$$\begin{aligned} \mathcal{H}_N^V(M, \alpha_S; M^2/\mu_R^2, M^2/\mu_F^2, M^2/Q^2) &= \sigma_V^{(0)}(M) \left[ 1 + \frac{\alpha_S}{\pi} \mathcal{H}_N^{V(1)}(M^2/\mu_F^2, M^2/Q^2) \right. \\ &\quad \left. + \left( \frac{\alpha_S}{\pi} \right)^2 \mathcal{H}_N^{V(2)}(M^2/\mu_R^2, M^2/\mu_F^2, M^2/Q^2) + \dots \right] , \quad (8) \end{aligned}$$

where  $\sigma_V^{(0)}$  is the partonic cross section at the Born level.

In the case of production of the DY lepton pair  $\ell \ell'$ ,  $\sigma_V^{(0)}$  is the electroweak cross section of the process  $q\bar{q} \rightarrow V \rightarrow \ell \ell'$ , and the corresponding first-order coefficients  $\mathcal{H}_{q\bar{q} \leftarrow ab, N}^{V(1)}$  in Eq. (8) are known [38]. They are:

$$\mathcal{H}_{q\bar{q} \leftarrow q\bar{q}, N}^{V(1)} = C_F \left( \frac{1}{N(N+1)} - 4 + \frac{\pi^2}{2} \right) - \left( B_q^{(1)} + \frac{1}{2} A_q^{(1)} \ln \frac{M^2}{Q^2} \right) \ln \frac{M^2}{Q^2} + 2\gamma_{qq, N}^{(1)} \ln \frac{Q^2}{\mu_F^2} , \quad (9)$$

$$\mathcal{H}_{q\bar{q} \leftarrow gq, N}^{V(1)} = \mathcal{H}_{q\bar{q} \leftarrow qg, N}^{V(1)} = \frac{1}{2(N+1)(N+2)} + \gamma_{qg, N}^{(1)} \ln \frac{Q^2}{\mu_F^2} , \quad (10)$$

$$\mathcal{H}_{q\bar{q} \leftarrow gg, N}^{V(1)} = \mathcal{H}_{q\bar{q} \leftarrow qq, N}^{V(1)} = \mathcal{H}_{q\bar{q} \leftarrow \bar{q}\bar{q}, N}^{V(1)} = 0 , \quad (11)$$

where  $\gamma_{ab, N}^{(1)}$  are the leading order (LO) anomalous dimensions. The second-order coefficients  $\mathcal{H}_{q\bar{q} \leftarrow ab, N}^{V(2)}$  for the DY process have not yet been computed.

We now turn to consider the finite component, of the cross section (see Eq. (2)). Since  $d\hat{\sigma}_{V ab}^{(\text{fin.})}$  does not contain large logarithmic terms, it can be computed by truncation of the perturbative series at a given fixed order (LO, NLO and so forth). This component is evaluated by starting from the usual perturbative truncation of the partonic cross section  $d\hat{\sigma}_{V ab}$  at a given order and subtracting the expansion of the resummed component  $d\hat{\sigma}_{V ab}^{(\text{res.})}$  at the *same* perturbative order (see Sect. 2.4 of Ref. [29]). Using this procedure, the resummed and fixed-order calculations are consistently matched by avoiding double-counting of perturbative contributions in the region of intermediate and large values of  $q_T$ .

The formalism that we have briefly recalled in this section defines a systematic ‘order-by-order’ (in extended sense) expansion [29] of Eq. (2): it can be used to obtain predictions that contain the full information of the perturbative calculation up to a given fixed order plus resummation of logarithmically-enhanced contributions from higher orders. The various orders of this expansion are denoted<sup>§</sup> as LL, NLL+LO, NNLL+NLO, etc., where the first label (LL, NLL, NNLL, ...) refers to the logarithmic accuracy at small  $q_T$  and the second label (LO, NLO, ...) refers to the customary perturbative order at large  $q_T$ . To be precise, the NLL+LO term of Eq. (2) is obtained by including the functions  $g^{(1)}$ ,  $g_N^{(2)}$  and the coefficient  $\mathcal{H}_N^{V(1)}$  in the resummed component, and by computing the finite (i.e. large- $q_T$ ) component at the LO (i.e. at  $\mathcal{O}(\alpha_S)$  for the DY process). At NNLL+NLO accuracy, the resummed component includes also the function  $g_N^{(3)}$  and the coefficient  $\mathcal{H}_N^{V(2)}$ , while the finite component is expanded up to NLO (i.e. at  $\mathcal{O}(\alpha_S^2)$  for the DY process). It is worthwhile noticing that the NLL+LO (NNLL+NLO) result includes the *full* NLO (NNLO)

---

<sup>§</sup>In the literature on  $q_T$  resummation, other authors sometime use the same labels (NLL, NLO and so forth) with a meaning that is different from ours.

perturbative contribution in the small- $q_T$  region. In particular, the NLO (NNLO) result for total cross section is exactly recovered upon integration over  $q_T$  of the differential cross section  $d\sigma/dq_T$  at NLL+LO (NNLL+NLO) accuracy.

In the case of the DY process, the second-order coefficient  $\mathcal{H}_N^{V(2)}$  is still unknown: this prevents us from performing calculations at NNLL+NLO accuracy. In the following we limit ourself to presenting results of calculations at NLL+LO accuracy<sup>¶</sup>.

We note that the inclusion of the function  $g_N^{(3)}$  and of the finite component at NLO is feasible at present. This procedure implements the complete NLO information at large  $q_T$ , but it does not lead to a consistent systematic improvement of the perturbative accuracy at small  $q_T$ . For instance, this procedure does not recover the total cross section at NNLO: the missing NNLO (i.e.  $\mathcal{O}(\alpha_S^2)$ ) contribution to the total cross section is due to  $\mathcal{H}_N^{V(2)}$ , and it is localized in the small- $q_T$  region. Moreover, starting from  $\mathcal{O}(\alpha_S^3)$ , the contribution  $\alpha_S g_N^{(3)}(\alpha_S L)$  in Eq. (6) and the missing contribution from the combined effect of  $\alpha_S^2 \mathcal{H}_N^{V(2)}$  and  $L g^{(1)}(\alpha_S L)$  (i.e.  $\alpha_S^2 \mathcal{H}_N^{V(2)} L g^{(1)}(\alpha_S L) = \alpha_S \mathcal{H}_N^{V(2)} \alpha_S L g^{(1)}(\alpha_S L)$ ) are of the same logarithmic order, namely, they are both NNLL contributions ( $\propto \alpha_S(\alpha_S L)^n$ ).

Within our formalism, the resummation factor  $\mathcal{W}_N^V(b, M)$  is directly defined, at fixed  $M$ , in the space of the conjugate variables  $N$  and  $b$ . To obtain the hadronic (partonic) cross section, as function of the kinematical variables  $s$  ( $\hat{s}$ ) and  $q_T$ , we have to perform inverse integral transformations. These integrals are carried out numerically. We recall [29] that the resummed form factor  $\exp\{\mathcal{G}_N(\alpha_S(\mu_R^2), \tilde{L})\}$  (more precisely, each of the functions  $g_N^{(i)}(\alpha_S \tilde{L})$  in Eq. (6)) is singular at the values of  $b$  where  $\alpha_S(\mu_R^2) \tilde{L} \geq \pi/\beta_0$  ( $\beta_0$  is the first-order coefficient of the QCD  $\beta$  function). When performing the inverse Fourier (Bessel) transformation with respect to the impact parameter  $b$  (see Eq. (3)), we deal with this singularity by using the regularization prescription of Refs. [47, 25]: the singularity is avoided by deforming the integration contour in the complex  $b$  space.

The singularity of the resummed form factor occurs at large values of the impact parameter:  $b \gtrsim 1/\Lambda_{QCD}$ , where  $\Lambda_{QCD}$  is the momentum scale of the Landau pole of the perturbative running coupling  $\alpha_S(q^2)/\pi \sim [\beta_0 \ln(q^2/\Lambda_{QCD}^2)]^{-1}$ . This singularity signals the onset of non-perturbative phenomena at very large values of  $b$  or, equivalently, in the region of very small transverse momenta. The regularization prescription that we use has to be regarded as a ‘minimal prescription’ [48, 47] within a purely perturbative framework. The prescription leaves unchanged the perturbative result to any (and arbitrarily-high) fixed order in  $\alpha_S$ , it does not require any infrared cut-off, and it can be implemented without introducing an explicit model of non-perturbative (NP) contributions. Owing to these features, the prescription is suitable to examine the perturbative effects and the ensuing perturbative uncertainty. This does not imply that NP contributions are small and can be neglected. We comment on NP effects at the end of Sect. 3.2.

### 3 $Z$ production at Tevatron energies: numerical results

In this section we present a selection of our numerical results, by considering the production of Drell–Yan  $e^+e^-$  pairs in  $p\bar{p}$  collisions at Tevatron energies. The numerical results are also compared

---

<sup>¶</sup> Perturbative information with comparable accuracy at small and intermediate values of  $q_T$  is implemented in the Monte Carlo event generators MC@NLO [44] and POWHEG [45, 46].

with the data collected by the CDF and D0 experiments at the energies  $\sqrt{s} = 1.8$  TeV (Run I) [49, 50] and  $\sqrt{s} = 1.96$  TeV (Run II, D0 only) [51].

As for the electroweak couplings, we use the scheme where the input parameters are  $G_F$ ,  $m_Z$ ,  $m_W$  and  $\alpha(m_Z)$ . In particular, we use the values  $G_F = 1.16639 \times 10^{-5}$  GeV<sup>-2</sup>,  $m_Z = 91.188$  GeV,  $m_W = 80.419$  GeV and  $\alpha(m_Z) = 1/128.89$ . Our calculation implements the decays  $\gamma^* \rightarrow e^+e^-$  and  $Z^* \rightarrow e^+e^-$  at fixed value of the invariant mass of the  $e^+e^-$  pair. In particular, we include the effects of the  $\gamma^* Z$  interference and of the finite width of the  $Z$  boson. Nonetheless, the numerical results of this section are obtained by simply using the narrow-width approximation and neglecting the photon contribution. We find that this approximation works to better than 1% accuracy in the inclusive regions of  $e^+e^-$  invariant mass that are covered by the CDF and D0 data. We recall that the measured  $q_T$  spectra are inclusive over the following ranges of  $e^+e^-$  invariant mass: 66–116 GeV [49], 75–105 GeV [50] and 70–110 GeV [51].

### 3.1 Fixed-order results

We start the presentation of the numerical results by considering QCD calculations at fixed order. To compute the LO and NLO hadronic cross section we use the MRST2002 LO [52] and MRST2004 NLO [53] parton distribution functions, with  $\alpha_S$  evaluated at 1 and 2 loops, respectively. As for renormalization and factorization scale, we choose  $\mu_F = \mu_R = m_Z$  as central value. The fixed-order predictions for the  $q_T$ -spectrum are obtained by using a numerical program that implements the analytical results of Refs. [6, 7, 8]. Similar numbers are obtained by using the Monte Carlo code of the MCFM package [54].

In Fig. 1 we plot the  $q_T$  spectrum of Drell–Yan  $e^+e^-$  pairs at the Tevatron Run I ( $\sqrt{s} = 1.8$  GeV) at LO and NLO accuracy. The bands are obtained by varying independently the factorization ( $\mu_F$ ) and renormalization ( $\mu_R$ ) scales in the range  $0.5m_Z \leq \mu_F, \mu_R \leq 2m_Z$ , with the constraint  $0.5 \leq \mu_F/\mu_R \leq 2$ . At the LO level, the scale dependence is about  $\pm 25\%$  at large  $q_T$ , it decreases as  $q_T$  decreases, and it becomes about  $\pm 15\%$  at  $q_T \sim 20$  GeV. The scale dependence at NLO is about  $\pm 8\%$  at  $q_T \sim 20$  GeV, with a slight reduction at large  $q_T$ . We note that the LO and NLO bands do not overlap in the region where  $q_T \lesssim 70$  GeV. This proves that, in this region of transverse momenta, the size of the band obtained through scale variations at LO definitely underestimates the theoretical uncertainty due to the missing NLO corrections.

The inset plot of Fig. 1 shows the  $K$ -factor, obtained by normalizing the NLO band with the LO result at  $\mu_F = \mu_R = m_Z$ . The impact of the NLO corrections, at central values of the scales, ranges from about  $+10\%$  at  $q_T \sim 200$  GeV to about  $+50\%$  at  $q_T \sim 20$  GeV.

In Fig. 2 we compare the results of the fixed-order calculations with CDF and D0 data. The experimental error bars reported in Fig. 2 include statistical and systematic contributions, but they do not include the overall normalization uncertainty due to the luminosity measurement. The CDF and D0 luminosity uncertainties are  $\pm 3.9\%$  and  $\pm 4.4\%$ , respectively. The corresponding cross sections are  $\sigma_{\text{CDF}} = 248 \pm 11$  pb [49] and  $\sigma_{\text{D0}} = 221 \pm 11$  pb [55], where the errors are dominated by the luminosity uncertainties. We note that, using the MRST2004 parton distribution functions [53] and including the effect of scale variations, the values of the QCD cross section at NLO and NNLO are  $\sigma_{\text{NLO}} = 226 \pm 5$  pb and  $\sigma_{\text{NNLO}} = 236 \pm 2$  pb, respectively.



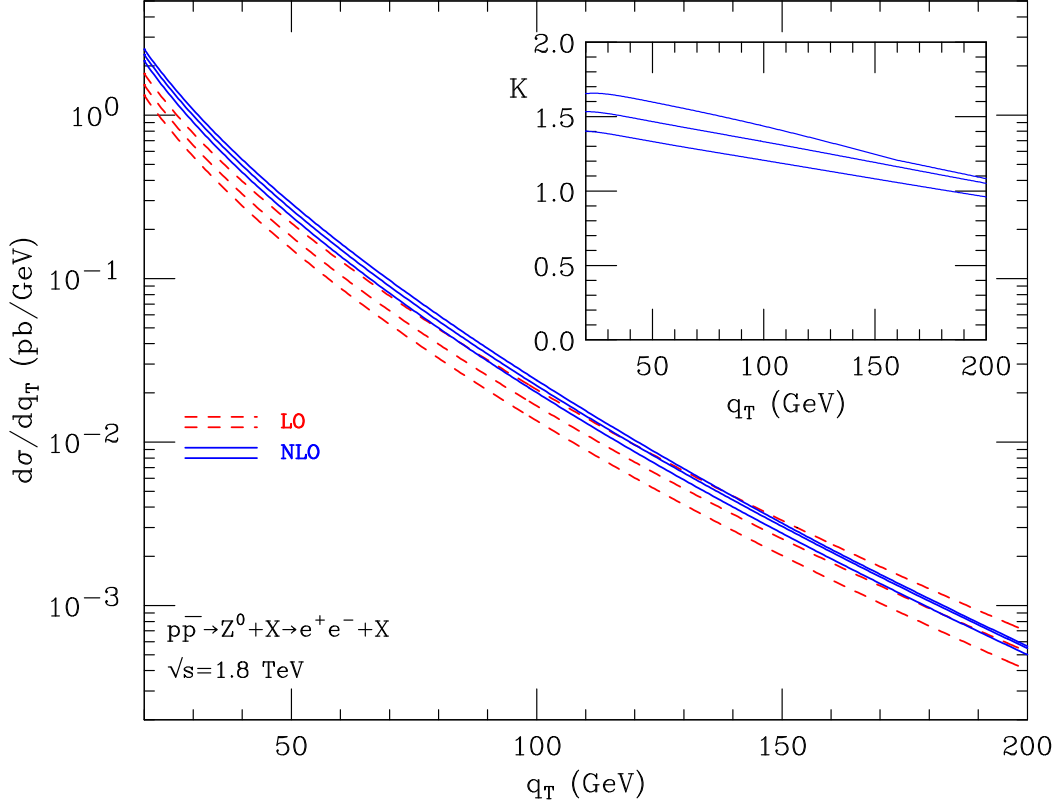


Figure 1: *The  $q_T$  spectrum of the Drell-Yan  $e^+e^-$  pairs produced in  $p\bar{p}$  collisions at the Tevatron Run I: theoretical predictions at LO (dashed lines) and NLO (solid lines). The inset plot shows the ratio  $K$  of the NLO and LO results.*

From Fig. 2 we see that the NLO result is in agreement with the experimental data over a wide region of transverse momenta, from large to relatively-small values of  $q_T$ . In particular, in the region  $20 \text{ GeV} \lesssim q_T \lesssim 70 \text{ GeV}$ , the sizeable increase of the LO result produced by the NLO corrections is important to achieve the agreement between the data and the NLO calculation. In the small  $q_T$  region, which is shown in the inset plot, the LO and NLO calculations do not describe the data. This is not unexpected since, when  $q_T \rightarrow 0$ , the LO and NLO cross section eventually diverges to  $+\infty$  and  $-\infty$ , respectively. This is the region where the effects of soft-gluon resummation are essential and have to be taken into account.

A more effective comparison between the fixed-order calculations and the data can be performed by considering the fractional difference  $(X - \text{theory})/\text{theory}$ . We choose the NLO result at central value of the scales as ‘reference theory’ and we define the following fractional difference (see Fig. 3):

$$\frac{(d\sigma/dq_T)_X - (d\sigma/dq_T)_{NLO}(\mu_F = \mu_R = m_Z)}{(d\sigma/dq_T)_{NLO}(\mu_F = \mu_R = m_Z)}, \quad (12)$$

where the label  $X$  refers to either the LO and NLO results, including scale variations (dashed and solid curves in Fig. 3), or the experimental data.

The perturbative QCD predictions at NLO have an associated theoretical uncertainty due to missing higher-order terms. By comparing the numerical results at LO and NLO, we can try to

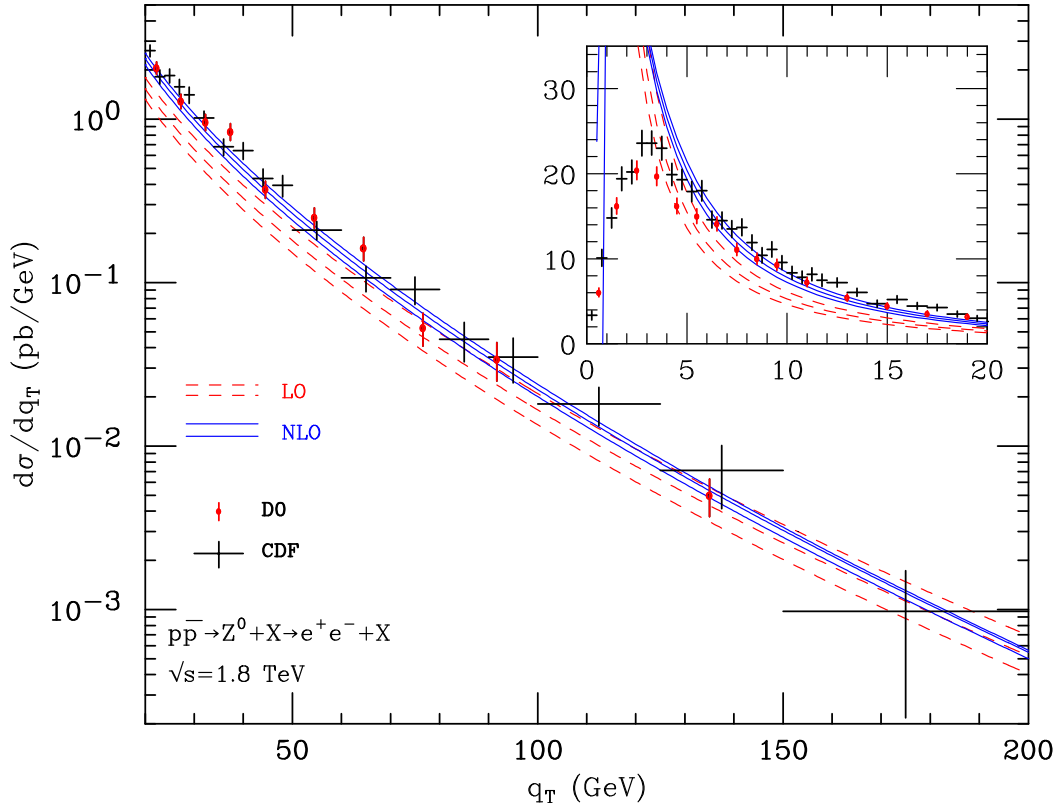


Figure 2: *The  $q_T$ -spectrum of the Drell-Yan  $e^+e^-$  pairs produced in  $p\bar{p}$  collisions at the Tevatron Run I. The data are from Refs. [49, 50]. Theoretical results are shown at LO (red dashed lines) and NLO (blue solid lines) including scale variations.*

consistently estimate this uncertainty. At large values of  $q_T$ , the LO and NLO bands overlap. In this region of transverse momenta, we can thus use the scale variation band as uncertainty estimate: we obtain that the NLO predictions have a perturbative uncertainty of about  $\pm 8\%$ . As  $q_T$  decreases below the value  $q_T \sim 70$  GeV, the LO and NLO bands do not overlap (see Fig. 3), and this signals that scale variations (up to NLO) tend to underestimate the effect of higher-order contributions. To obtain a more reliable estimate of the uncertainty of the NLO central value, we assign it a theoretical error as given by its difference with respect to its closest value in the LO band (i.e., the value on the upper curve of the LO band in Fig. 3). Using this procedure, we obtain a NLO uncertainty that increases as  $q_T$  decreases, and that reaches the value of about  $\pm 20\%$  at  $q_T \sim 20$  GeV. In the region of smaller values of  $q_T$ , the LO and NLO results show a pathological behaviour. This behaviour, which is discussed below, prevents us from making a sensible quantitative estimate of the theoretical uncertainty of the NLO predictions. We can only draw a qualitative conclusions: the uncertainty of the NLO predictions systematically increases as  $q_T$  decreases.

We know that, in the small- $q_T$  region, the convergence of the fixed-order perturbative expansion is spoiled by the presence of large logarithmic corrections. This behaviour is clearly seen in Fig. 3 by comparing the LO and NLO results at  $q_T \sim 1$  GeV. We also recall that, as  $q_T \rightarrow 0$ , the LO cross section diverges to  $+\infty$  whereas the NLO cross section diverges to  $-\infty$ . Since the NLO corrections increase the LO results at large  $q_T$ , the LO and NLO cross sections have to coincide at

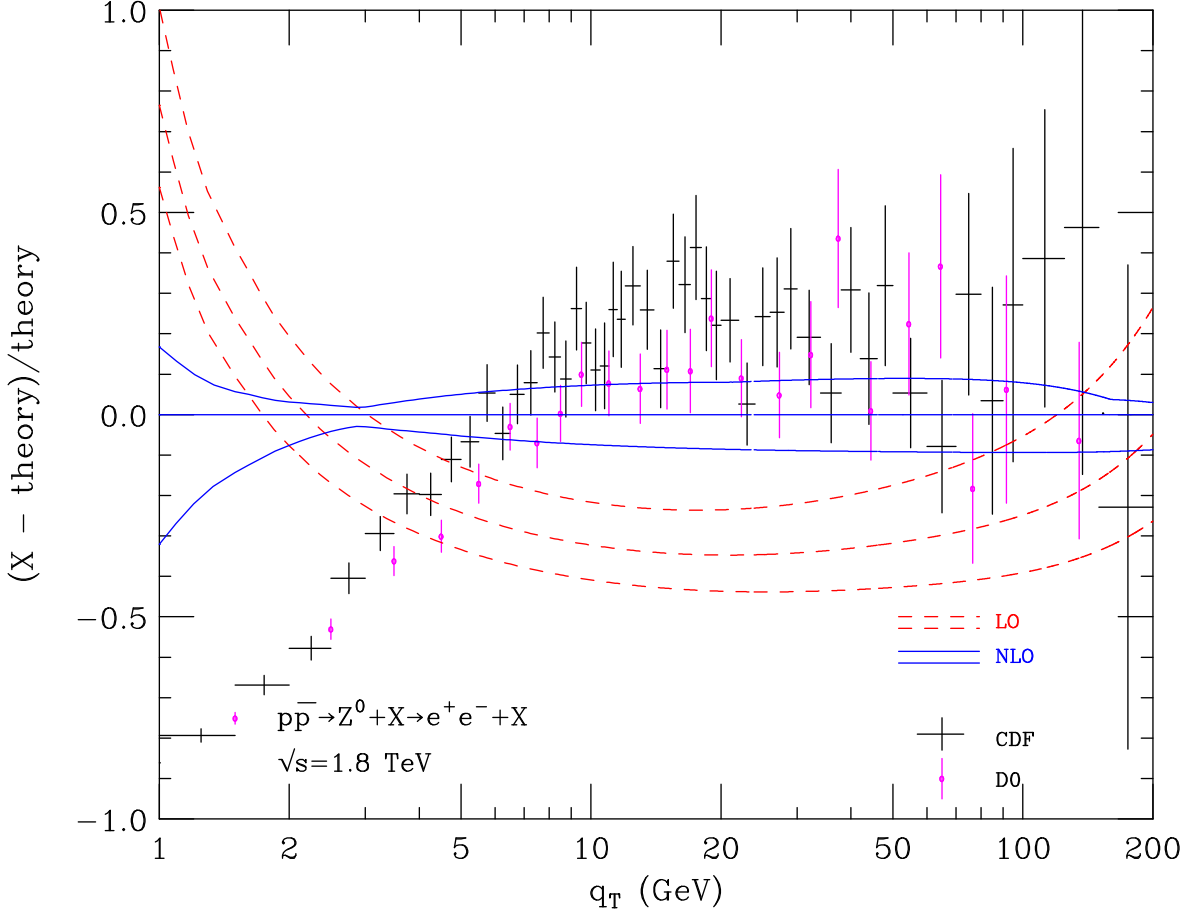


Figure 3: *Fractional difference of fixed-order predictions and Tevatron Run I data with respect to the NLO result at  $\mu_F = \mu_R = m_Z$  (see Eq. (12)).*

some intermediate value of  $q_T$ , before reaching the small- $q_T$  region where their different divergent behaviour sets in. The numerical agreement of the LO and NLO results occurs in the region where  $q_T \sim 2\text{--}3$  GeV (Fig. 3). Since this region is so close to that where the convergence of the fixed-order is definitely spoiled, it cannot be regarded as a region where the order-by-order expansion is well-behaved. Therefore, the systematic decrease of the difference between the LO and NLO cross sections when  $q_T$  varies from about 20 GeV to 2–3 GeV is simply driven by the sickness of the LO and NLO results at smaller  $q_T$ . This decrease cannot be interpreted as an increase of the theoretical accuracy of the NLO predictions. The behaviour of the LO and NLO results below  $q_T \sim 20$  GeV signals the necessity to include the effect of higher-order contributions and, eventually, of resummed calculations.

Having estimated the perturbative uncertainty of the NLO predictions, we can add some comments on the comparison with the experimental data (see Fig. 3). We consider the region where  $q_T \gtrsim 20$  GeV, since at smaller values of  $q_T$  the NLO calculation loses predictivity. Throughout this region, the data agree with the NLO predictions. The experimental errors are typically larger (smaller) than the NLO uncertainty when  $q_T \gtrsim 70$  GeV ( $20 \text{ GeV} \lesssim q_T \lesssim 30 \text{ GeV}$ ). The experimental errors and the corresponding NLO errors overlap, with the sole exception of a couple of D0 data points. We note that part of the differences between data and theory have a systematic component

due to the luminosity uncertainties ( $\pm 3.9\%$  at CDF, and  $\pm 4.4\%$  at D0) and to the values of the total cross sections. The NLO predictions for  $d\sigma/dq_T$  correspond to the value<sup>||</sup>  $\sigma = 233$  pb of the total cross section; this value is about 6% smaller than the CDF value, and it is about 5% larger than the D0 value. Therefore, by inspection of Fig. 3, we see that considering the normalized distribution  $\frac{1}{\sigma} \frac{d\sigma}{dq_T}$  (i.e. the shape of the  $q_T$  spectrum) would lead to an overall improvement of the agreement between the CDF data, the D0 data and the NLO predictions.

The D0 collaboration has performed a measurement [51] of the normalized  $q_T$  distribution,  $\frac{1}{\sigma} \frac{d\sigma}{dq_T}$ , from data at the Tevatron Run II ( $\sqrt{s} = 1.96$  GeV). To obtain fixed-order QCD predictions for the normalized distribution, we have to consistently compute  $d\sigma/dq_T$  and  $\sigma$ . The cross section  $d\sigma/dq_T$  at NLO (LO) is computed by convoluting the corresponding NLO (LO) partonic cross sections with NLO (LO) parton distributions. These differential partonic cross sections at NLO (LO) contribute to the total partonic cross sections at NNLO (NLO). Therefore, to normalize  $d\sigma/dq_T$  at NLO (LO), the total cross section  $\sigma$  is computed by convoluting the total partonic cross sections at NNLO (NLO) with NLO (LO) parton distributions. In conclusion, our fixed-order calculations of the normalized  $q_T$  distribution are obtained by using the following relation:

$$\left( \frac{1}{\sigma} \frac{d\sigma}{dq_T} \right)_{(N)LO}(\mu_F, \mu_R) \equiv \frac{1}{\sigma_{(N)NLO}(\mu_F, \mu_R)} \left( \frac{d\sigma}{dq_T} \right)_{(N)LO}(\mu_F, \mu_R) , \quad (13)$$

where the two factors,  $1/\sigma$  and  $d\sigma/dq_T$ , on the right-hand side are evaluated with the same parton distributions and at the same values of the renormalization and factorization scales.

The D0 data and the LO and NLO results for the normalized distribution  $\frac{1}{\sigma} \frac{d\sigma}{dq_T}$  at the Tevatron Run II are presented in Fig. 4. The LO and NLO bands are obtained by varying  $\mu_F$  and  $\mu_R$  in the same range as in the fixed-order calculations at Run I. The fractional difference  $(X - \text{theory})/\text{theory}$  at Run II is shown in Fig. 5; this fractional difference differs from that in Eq. (12) by the sole replacement of  $\frac{d\sigma}{dq_T}$  with  $\frac{1}{\sigma} \frac{d\sigma}{dq_T}$ .

Comparing Figs. 2 and 3 with Figs. 4 and 5, we can see that the overall features of the fixed-order results are unchanged in going from Run I to Run II. The main quantitative differences are due to the fact that, at Run II, we are considering the normalized  $q_T$  distribution. The NLO corrections to  $\frac{1}{\sigma} \frac{d\sigma}{dq_T}$  are smaller than the NLO corrections to  $\frac{d\sigma}{dq_T}$ . The scale dependence of the fixed-order results is only marginally reduced by considering  $\frac{1}{\sigma} \frac{d\sigma}{dq_T}$  rather than  $\frac{d\sigma}{dq_T}$ .

The perturbative uncertainty of the NLO predictions at Run II can be estimated in the same way as at Run I. We conclude that the NLO error increases from about  $\pm 6-8\%$  in the region where  $q_T \gtrsim 50$  GeV (see the size of the NLO band in Fig. 5) to about  $\pm 15\%$  at  $q_T \sim 20$  GeV (see the upper value of the LO band in Fig. 5). At smaller values of  $q_T$  the NLO calculation loses predictivity. In the region where  $q_T \gtrsim 90$  GeV, the D0 data agree with the NLO predictions. In the region where  $20 \text{ GeV} \lesssim q_T \lesssim 90 \text{ GeV}$ , the experimental errors are typically smaller than the NLO uncertainty; in this region, three data points overshoot the NLO predictions (they differ by about two standard deviations from the upper value of the NLO uncertainty band).

We add a comment on the fixed-order calculations presented in the papers of the D0 collaboration. The labels ‘‘Fixed-order ( $\mathcal{O}(\alpha_s^2)$ )’’ in Ref. [50] and ‘‘NNLO’’ in Ref. [51] refer to perturbative

---

<sup>||</sup>This value is obtained by convoluting the NNLO partonic cross sections with NLO parton distributions (see the comment above Eq. (13)).

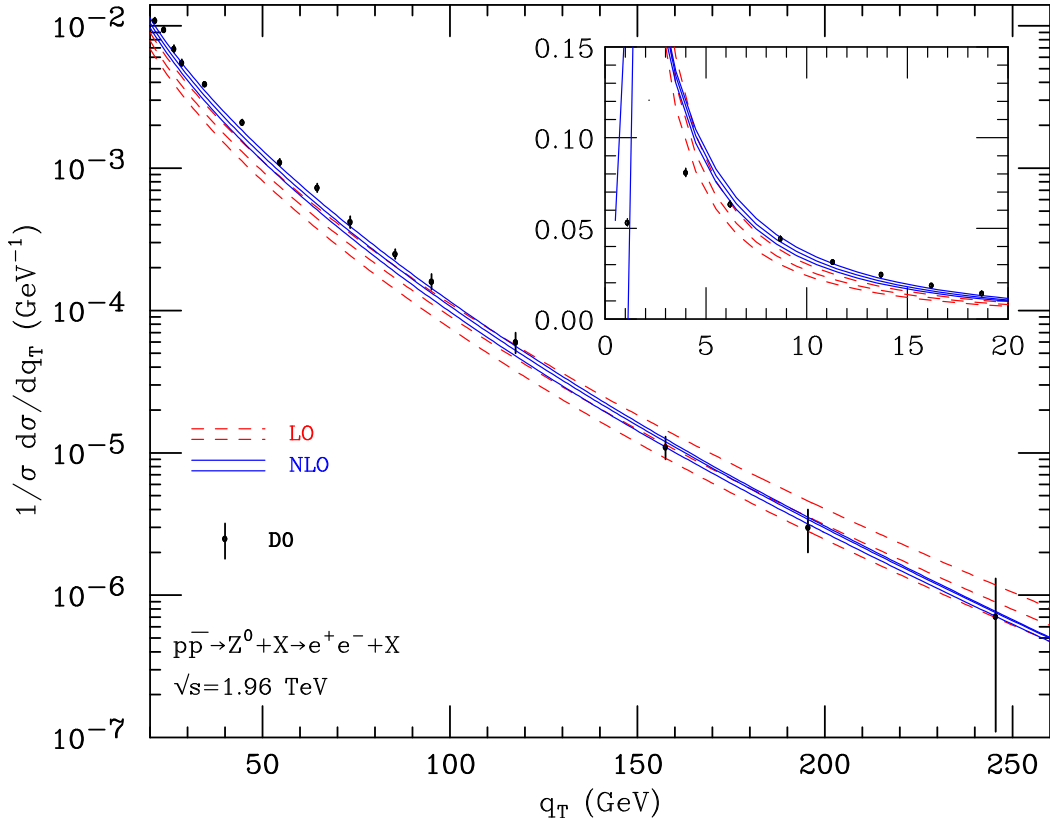


Figure 4: *The  $q_T$ -spectrum of the Drell-Yan  $e^+e^-$  pairs produced in  $p\bar{p}$  collisions at the Tevatron Run II, normalized to the total cross section. The data are from Ref. [51]. Theoretical results are shown at LO (red dashed lines) and NLO (blue solid lines) including scale variations.*

calculations that use the same NLO partonic cross sections of our NLO calculations. The differences between these calculations can be due to the use of different parton distributions and of different renormalization and factorization scales. In the region where  $q_T \gtrsim 20$  GeV, the fixed-order results of Refs. [50, 51] are systematically smaller than our NLO central values: the differences can reach the level of about 12% in the case of the “Fixed-order ( $\mathcal{O}(\alpha_s^2)$ )” result (compare Fig. 26 of the second paper in Ref. [50] with our Fig. 3) and of about 7% in the case of the “NNLO” result (compare Fig. 2b in Ref. [51] with our Fig. 5). We note that the differences tend to reduce the agreement with the D0 data; we also note that these differences are consistent with our estimate of the perturbative uncertainty of the NLO predictions. This observation underlines the relevance of quantifying the uncertainty of the perturbative QCD predictions.

### 3.2 Resummed results

In the following we present our resummed results at NLL+LO accuracy and we compare them with the Tevatron data. To compute the hadronic cross sections, we use the MRST2004 NLO parton distributions [53], with  $\alpha_s$  evaluated at 2-loop order.

In the small- $q_T$  region, the use of NLO parton distributions is fully consistent with the NLL+LO

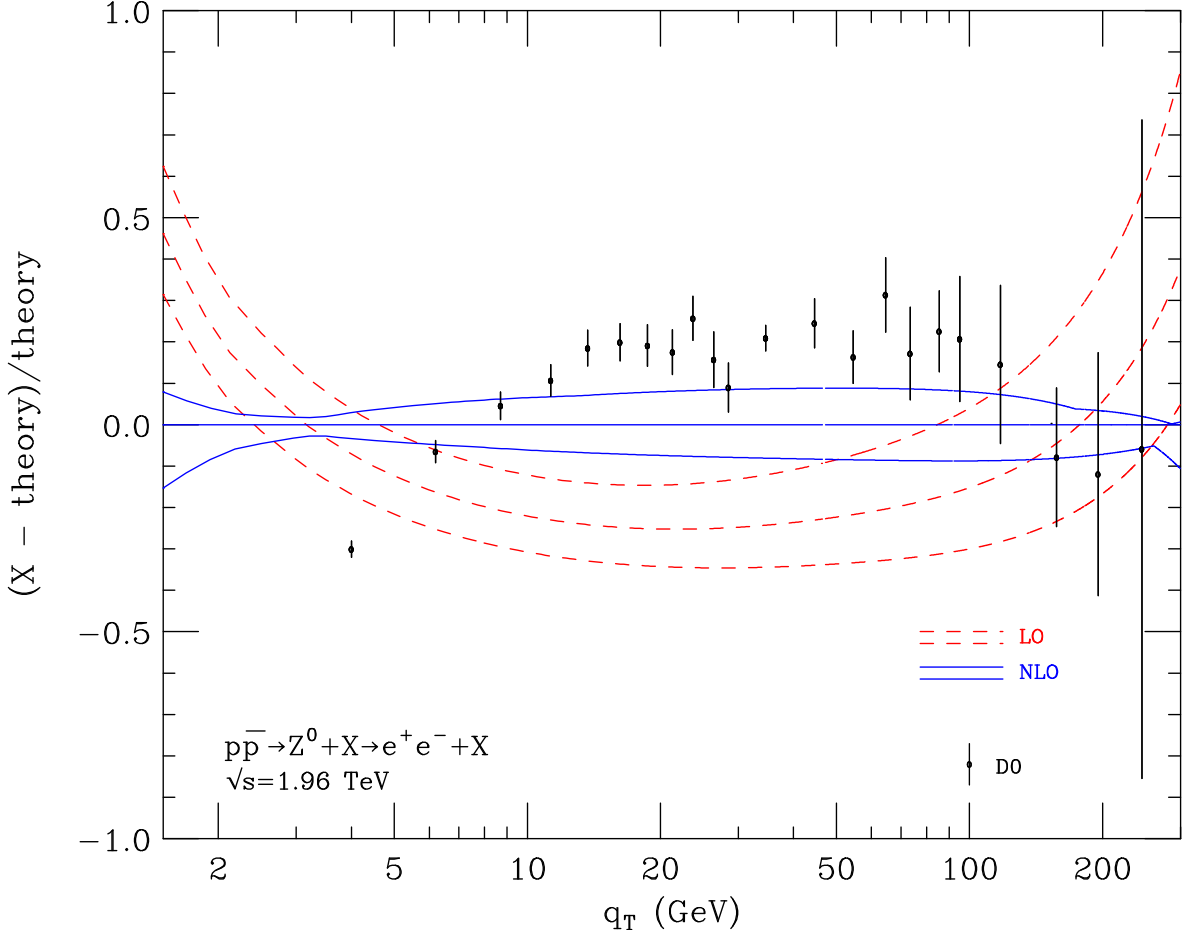


Figure 5: *Same as Fig. 3 for  $1/\sigma (d\sigma/dq_T)$  at the Tevatron Run II.*

accuracy of the partonic cross section. Indeed, at small values of  $q_T$ , the NLL+LO partonic cross section includes the complete perturbative expansion up to NLO (i.e.,  $\mathcal{O}(\alpha_S)$ ) and the resummation of the LL and NLL terms. The use of NLO parton distributions is justified also at intermediate values of  $q_T$ , where the calculation of the partonic cross section is driven by the small- $q_T$  resummation and constrained by the value of the total cross section at NLO.

The resummed calculation depends on the factorization and renormalization scales and on the resummation scale  $Q$ . As in fixed-order calculations, we choose  $\mu_F = \mu_R = m_Z$  as central value. Factorization and renormalization scale uncertainties are computed as described in Sect. 3.1, by considering variations of  $\mu_F$  and  $\mu_R$  by a factor of two around (above and below) the central value. A similar procedure is applied to the resummation scale: we choose  $Q = m_Z/2$  as central value and consider scale variations in the range  $m_Z/4 < Q < m_Z$ . As discussed below, we regard this central value of the resummation scale and the corresponding range  $m_Z/4 < Q < m_Z$  as sufficiently conservative (e.g., more conservative than the range  $m_Z/2 < Q < 2m_Z$ ) from a theoretical viewpoint<sup>†</sup>.

<sup>†</sup>Also in the case of Higgs boson production, we used [29] the range  $m_H/4 < Q < m_H$  ( $m_H$  being the mass of the Higgs boson) to estimate the resummation scale uncertainty.

The resummed logarithmic terms depend on  $Q$  through the variable  $\tilde{L}$  in Eq. (7). This implies that the logarithmic contributions are mostly effective in the  $b$ -space region where  $bQ \gtrsim 1$ , which corresponds to the transverse-momentum region where  $q_T \lesssim Q$ . By decreasing  $Q$ , the resummation effects are depleted in the region where  $q_T \gtrsim Q$  and enhanced in the region where  $q_T \lesssim Q$ . The bulk of the  $Z$  production cross section and, thus, the main effect of the logarithmic terms are located at values of  $q_T$  that are certainly smaller than  $m_Z$ : indeed, we observe that the average transverse momentum of the  $Z$  boson is of the order of  $\alpha_S(m_Z) m_Z$ . Therefore, it is physically sensible to use a central value of  $Q$  that is smaller than  $m_Z$ . Nonetheless, too small values of  $Q$  have to be avoided. As we have pointed out in Sect. 3.1, the fixed-order perturbative expansion shows instabilities (due to higher-order logarithmic corrections) in the region where  $q_T \lesssim 20$  GeV. Therefore, in our NLL+LO calculation we should exclude values of  $Q$  that are smaller than about 20 GeV. In this respect, a value of  $Q$  as low as  $Q \sim m_Z/4$  can be regarded as a conservative value from a perturbative viewpoint. The NLL+LO calculation with such a value of  $Q$  will be closer to the corresponding fixed-order calculation throughout region of intermediate values of  $q_T$  where the fixed-order expansion is relatively well behaved.

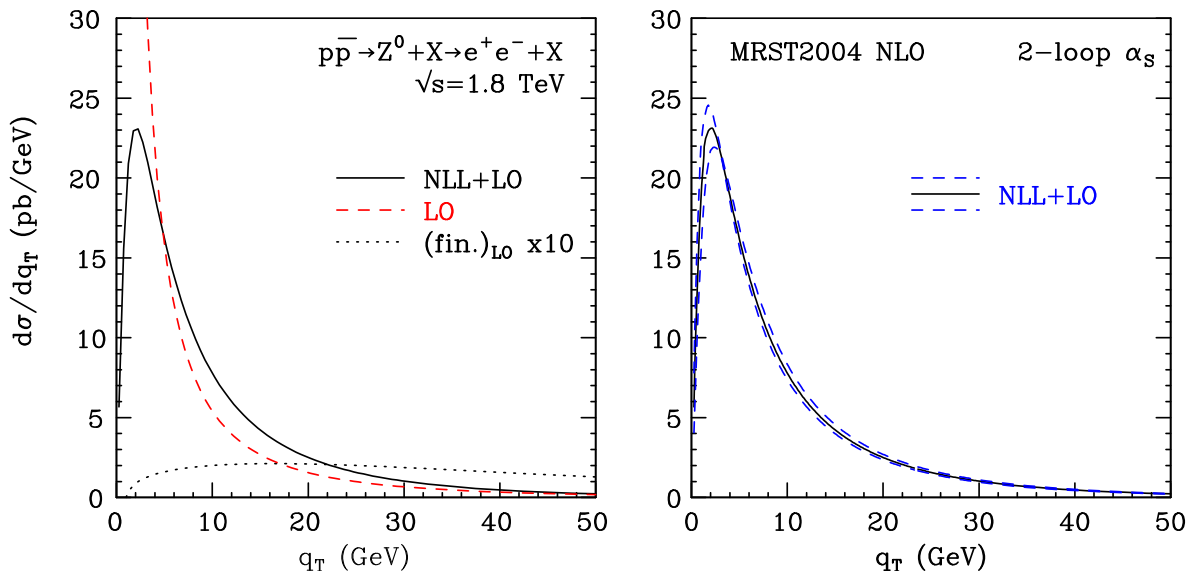


Figure 6: *The NLL+LO  $q_T$  spectrum at the Tevatron Run I.*

The NLL+LO  $q_T$  spectrum at the Tevatron ( $\sqrt{s} = 1.8$  TeV) is presented in Fig. 6. In the left panel, the NLL+LO result (solid line) at the default scales ( $\mu_F = \mu_R = m_Z$ ,  $Q = m_Z/2$ ) is compared with the corresponding <sup>‡</sup> LO result (dashed line). We observe that soft-gluon resummation leads to a well-behaved distribution: it vanishes as  $q_T \rightarrow 0$ , has a kinematical peak at  $q_T \sim 2$  GeV, and tends to the corresponding LO result at larger values of  $q_T$ . The LO finite component of the spectrum (see Eq. (2)), rescaled by a factor of 10 to make it more visible, is also shown for comparison (dotted line). This component smoothly vanishes as  $q_T \rightarrow 0$  and gives a small contribution to the NLL+LO result in the low- $q_T$  region. The contribution is smaller than

<sup>‡</sup>Here and in the inset plot of Figs. 8, the LO result refers to the convolution of the partonic cross section at LO with the parton distributions at NLO. This LO result thus differs from the customary LO calculation, which uses parton distributions at LO and is presented in Sect. 3.1. Incidentally, we note that the difference produced by using NLO vs. LO parton distributions is much smaller than the scale uncertainty of the corresponding results. We find that the difference is below the level of about  $\pm 2\%$  ( $-6\%$ ) if  $20 \text{ GeV} \lesssim q_T \lesssim 140 \text{ GeV}$  ( $140 \text{ GeV} \lesssim q_T \lesssim 200 \text{ GeV}$ ).

1% at the peak and becomes more important as  $q_T$  increases: it is about 8% at  $q_T \sim 20$  GeV, about 20% at  $q_T \sim 30$  GeV and about 60% at  $q_T \sim 50$  GeV. A similar quantitative behaviour is observed by considering the contribution of the LO finite component to the LO result; the contribution is about 13% at  $q_T \sim 20$  GeV, about 30% at  $q_T \sim 30$  GeV and about 75% at  $q_T \sim 50$  GeV. In the region of intermediate values of  $q_T$  (say, around 20 GeV), the difference between the NLL+LO and LO results is much larger than the size of the LO finite component. This difference is produced by the logarithmic terms (at NLO and beyond NLO) that are included in the resummed calculation at NLL accuracy. At large values of  $q_T$  the contribution of the LO finite component sizeably increases. This behaviour indicates that the logarithmic terms are no longer dominant and that the resummed calculation cannot improve upon the predictivity of the fixed-order expansion.

In the right panel of Fig. 6 we show the scale dependence of the NLL+LO result. The band (dashed lines) is obtained by varying the renormalization and factorization scales as described in Sect. 3.1. Although  $\mu_R$  and  $\mu_F$  are varied independently, we find that the dependence on  $\mu_R$  dominates at any values of  $q_T$ . In the region of small and intermediate values of  $q_T$ , the scale dependence of the NLL+LO result is definitely much smaller than the difference between the NLL+LO and LO results. The scale dependence of the resummed result is about  $\pm 5\%$  at the peak, and it increases to  $\pm 9\%$  at  $q_T \sim 50$  GeV.

The renormalization/factorization scale dependence of the NLL+LO spectrum (the band enclosed by the solid lines) is more clearly visible in Fig. 7. Here the CDF and D0 data at Tevatron Run I are also superimposed on the NLL+LO result. There is an overall agreement between the data and the resummed calculation in the region from small to intermediate values of  $q_T$ . In particular, the agreement tends to improve by decreasing the value of  $\mu_R$  from  $\mu_R = m_Z$  to  $\mu_R = m_Z/2$ . The inset plot shows the region of intermediate and large values of  $q_T$ . At large  $q_T$ , the NLL+LO result deviates from the data, and the deviation increases as  $q_T$  increases. As previously observed on purely theoretical grounds, the NLL+LO calculation loses predictivity in the large- $q_T$  region. The loss of predictivity is also signalled by the systematic increase of the scale dependence, whose size is about  $\pm 9\%$  at  $q_T \sim 50$  GeV and becomes about  $\pm 22\%$  at  $q_T \sim 90$  GeV. As we shall see in the next figure, at large values of  $q_T$ , the dependence on the resummation scale  $Q$  is even stronger than the dependence on  $\mu_R$  and  $\mu_F$ .

In Fig. 8 we show how the NLL+LO result depends on the resummation scale  $Q$ . We fix  $\mu_R = \mu_F = m_Z$ , and we present the result of the NLL+LO calculation at three different values of the resummation scale:  $Q = m_Z$  (dashed line),  $Q = m_Z/2$  (solid line) and  $Q = m_Z/4$  (dot-dashed line). In the region of small and intermediate values of  $q_T$ , large values of  $Q$  ( $Q \sim m_Z, m_Z/2$ ) lead to a better agreement with the experimental data. In this region, the  $q_T$  spectrum at NLL+LO becomes softer by decreasing the value of  $Q$ . This behaviour is not unexpected. The resummed calculation cures the instabilities of the fixed-order calculations by implementing the physical transverse-momentum smearing produced by soft multiparton radiation. The size of the  $q_T$  region where the smearing takes place is controlled by the value of  $Q$ . By increasing  $Q$ , the resummation smearing is extended to larger values of  $q_T$ , and the  $q_T$  spectrum becomes harder.

The inset plot of Fig. 8 refers to the region of intermediate and large values of  $q_T$ . We present the NLL+LO results and the corresponding LO result (dotted line), which does not depend on  $Q$ . Considering large values of  $Q$  ( $Q \sim m_Z, m_Z/2$ ), the NLL+LO results follow the data up to  $q_T \sim 50$  GeV and deviates from the data at larger values of  $q_T$ . At large  $q_T$ , the deviation decreases if we consider the NLL+LO calculation with smaller values of  $Q$ . We also notice that



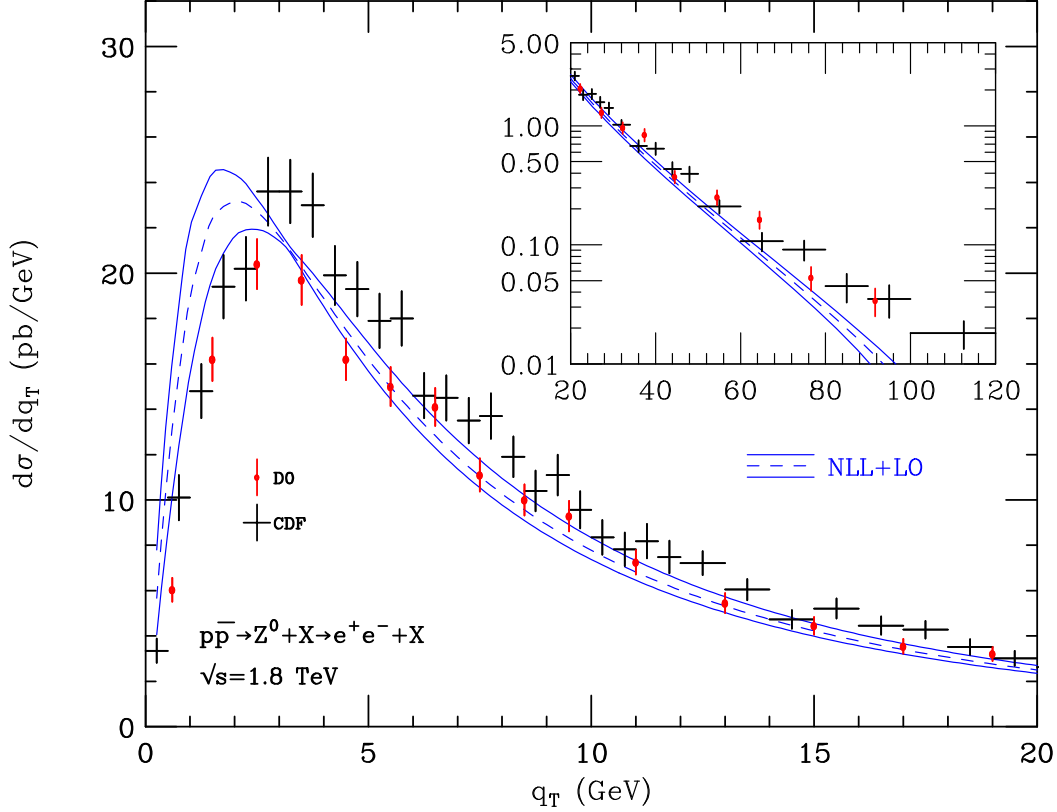


Figure 7: Comparison of Tevatron Run I data with the NLL+LO result including variations of the scales  $\mu_F$  and  $\mu_R$ .

the LO result is approximated better by the NLL+LO calculation if  $Q$  is smaller. This fact is not surprising. Varying  $Q$ , we smoothly set the transverse-momentum scale below which the resummed logarithmic terms are mostly effective; if  $Q$  is smaller, the resummation effects are confined to a range of smaller values of  $q_T$ . Independently of these observations, the sizeable  $Q$  dependence of the resummed calculation at large  $q_T$  confirms the lost of predictivity of the NLL+LO result in this transverse-momentum region.

The variations of the NLL+LO cross section produced by varying the resummation scale give further insight on the size of yet uncalculated higher-order logarithmic contributions at small and intermediate values of  $q_T$ . To quantify the resummation scale uncertainty on the cross section, we choose  $Q = m_Z/2$  as central value and vary  $Q$  between  $m_Z$  and  $m_Z/4$ . We find that the uncertainty is about  $\pm 12\%$  in the region of the peak, it decreases in the region around  $q_T \sim 5$  GeV, and then it increases to about  $\pm 15\%$  in the region where  $q_T \sim 20$  GeV.

The integral over  $q_T$  of the NLL+LO spectrum is in agreement (for any values of  $\mu_R, \mu_F$  and  $Q$ ) with the value of the NLO total cross section to better than 1%, thus checking the numerical accuracy of our code. We also note that the large- $q_T$  region gives a little contribution to the total cross section; therefore, the total cross section constraint mainly acts as a perturbative constraint on the NLL+LO spectrum in the region from intermediate to small values of  $q_T$ . To confirm this statement at the quantitative level, we consider the cross section ratio  $\sigma(q_{T_{\max}})/\sigma$ , where  $\sigma(q_{T_{\max}})$  is the contribution to the total cross section  $\sigma$  from the transverse-momentum

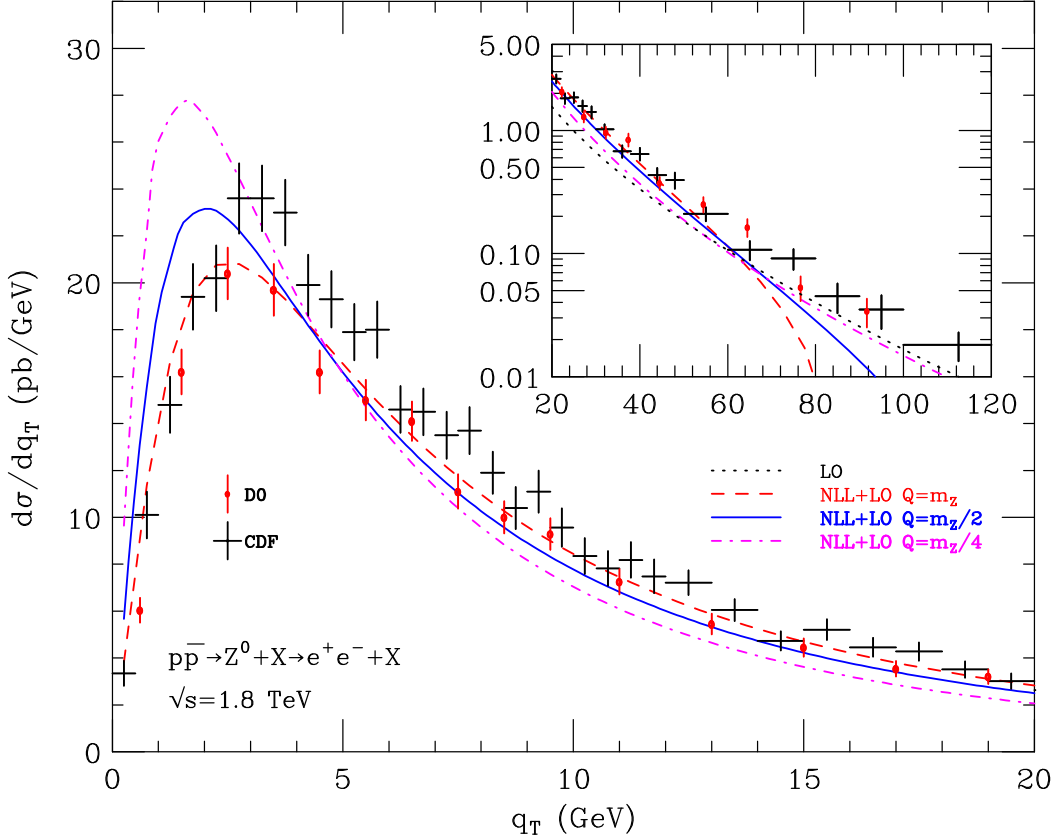


Figure 8: *NLL+LO results at the Tevatron Run I for different values of the resummation scale  $Q$ .*

region where  $q_T \leq q_{T\max}$ . The cross section  $\sigma(q_{T\max})$  can be computed either at the NLO or at NLL+LO accuracy (i.e. by integration of the NLL+LO spectrum over  $q_T$ ). Provided  $q_{T\max}$  is not small, we find that the NLO and NLL+LO values of  $\sigma(q_{T\max})$  are very close and that  $\sigma(q_{T\max})$  constitutes a large fraction of  $\sigma$ . For example, the NLO (NLL+LO) value of the cross section ratio is  $\sigma(q_{T\max})/\sigma = 0.86$  (0.87) at  $q_{T\max} = 20$  GeV and  $\sigma(q_{T\max})/\sigma = 0.93$  (0.94) at  $q_{T\max} = 30$  GeV. The resummation scale uncertainty of  $\sigma(q_{T\max})$  at NLL+LO accuracy is about  $\pm 2\%$  at  $q_{T\max} = 20$  GeV, and it is below the 1% level in the region where  $q_{T\max} \gtrsim 30$  GeV.

In analogy with our presentation of the fixed-order results in Sect. 3.1, we consider the resummed results and introduce a corresponding fractional difference  $(X - \text{theory})/\text{theory}$ . Now, at variance with Eq. (12), we choose the NLL+LO result at central value of the scales as ‘reference theory’ and we define the following fractional difference:

$$\frac{(d\sigma/dq_T)_X - (d\sigma/dq_T)_{NLL+LO}(\mu_F = \mu_R = 2Q = m_Z)}{(d\sigma/dq_T)_{NLL+LO}(\mu_F = \mu_R = 2Q = m_Z)}, \quad (14)$$

where the label  $X$  refers to either the experimental data or the NLL+LO result at various values of the scales.

This fractional difference is shown in Fig. 9. The band enclosed by the solid lines corresponds to our computation of the scale uncertainty. It includes the combined effect from varying  $\mu_F, \mu_R$

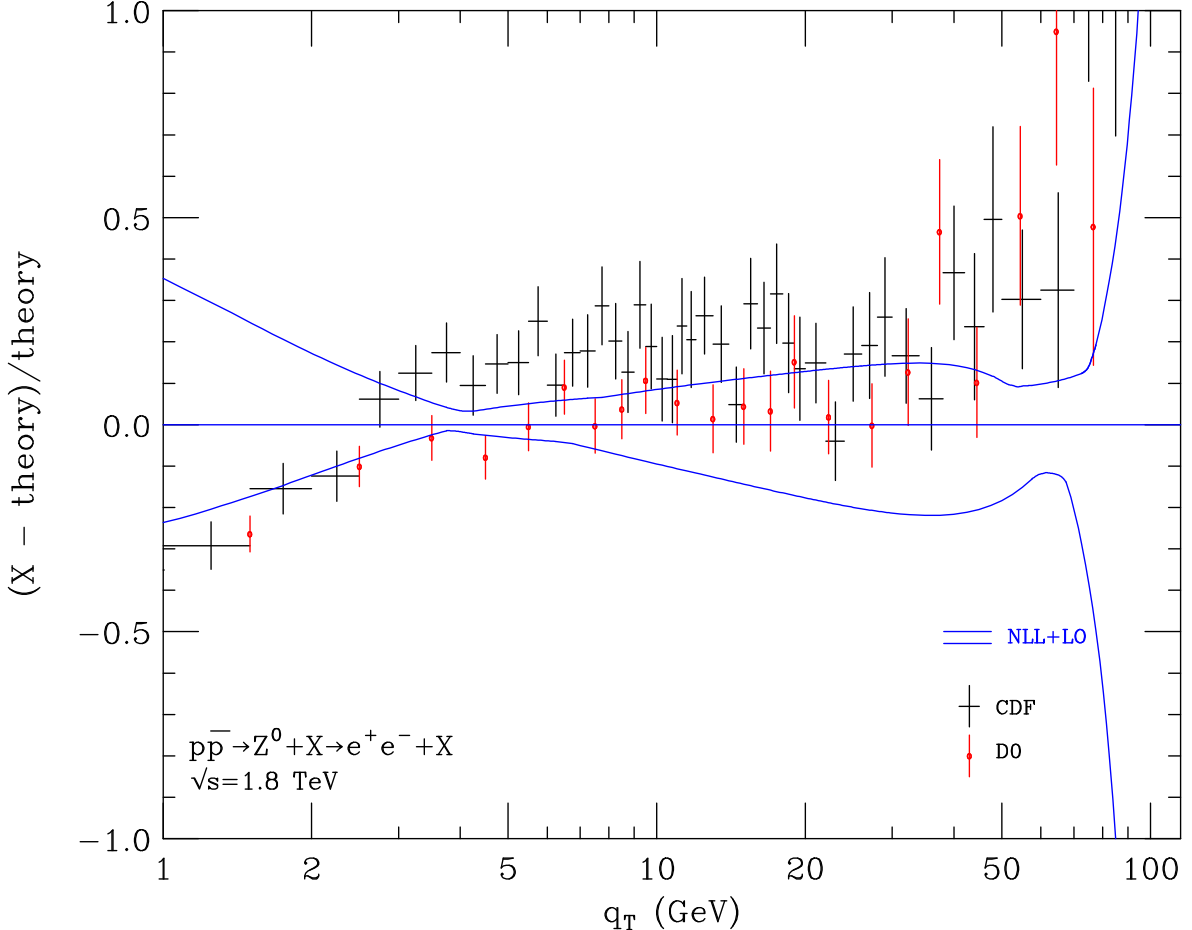


Figure 9: *Fractional difference of Tevatron data with respect to the NLL+LO prediction at  $\mu_F = \mu_R = 2Q = m_Z$  (see Eq. (14)). The band represents the combined effect of varying the scales as described in the text.*

and  $Q$  as previously described. We find that the resummation scale uncertainty is larger than the factorization/renormalization scale uncertainty at (almost) all values of  $q_T$ . We comment on the results in Fig. 9 by considering various regions of transverse momenta in turn.

We first consider the large- $q_T$  region. At  $q_T \sim 40$  GeV, the scale uncertainty of the NLL+LO result is of about  $\pm 20\%$ . At high  $q_T$ , the scale uncertainty is definitely larger and quickly increases as  $q_T$  increases. The decrease of the scale uncertainty in the region around  $q_T \sim 60$  GeV has no physical interpretation: it has to be regarded as an accidental fact rather than a reduction of the theoretical uncertainty. Comparing the uncertainty of the NLL+LO calculation with that of the fixed-order calculations (see Sect. 3.1), we thus conclude that, in the large- $q_T$  region, the NLL+LO predictions are less accurate than the NLO predictions.

In the region of intermediate values of  $q_T$ , the scale uncertainty of the NLL+LO result is moderate (see Fig. 9). In this region it is appropriate to perform a more detailed comparison between the NLL+LO calculation and the fixed-order calculations. We consider Eq. (12), which uses the NLO central value as ‘reference theory’, and we compute the fractional difference of the NLL+LO calculation. The results are presented in Fig. 10, which shows the NLL+LO calculation

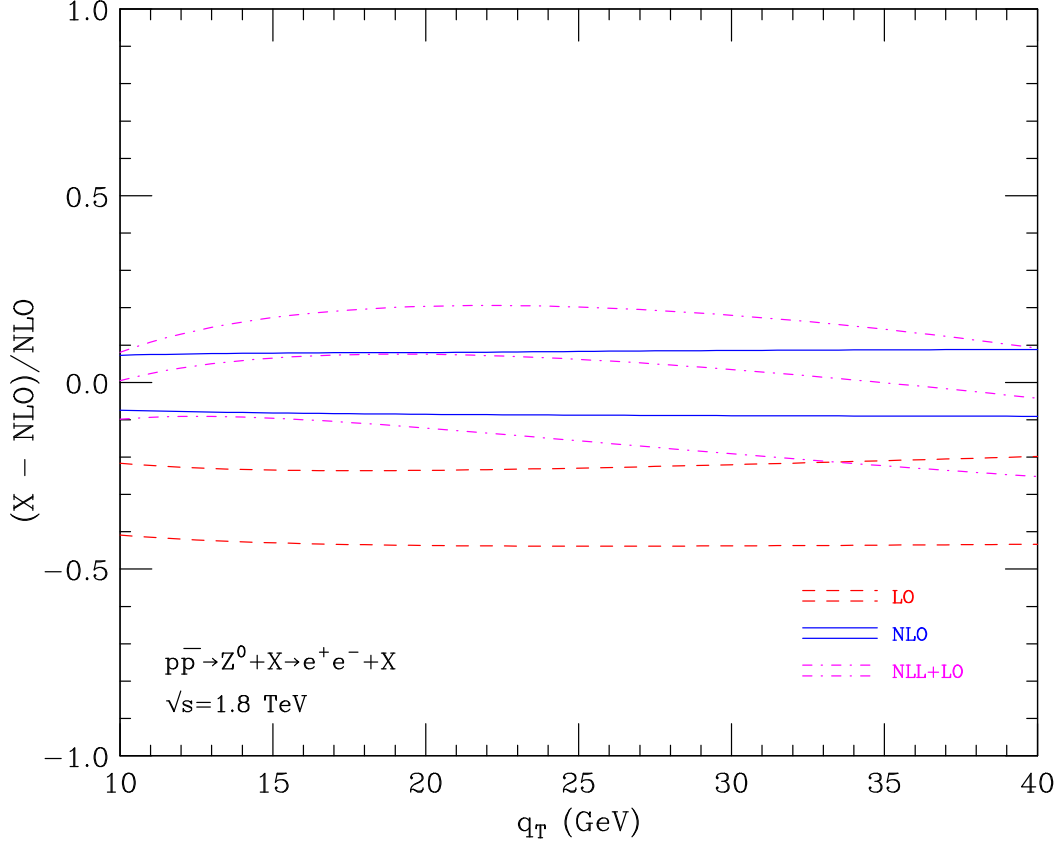


Figure 10: *Fractional difference of LO (dashed), NLO (solid) and NLL+LO (dot dashed) predictions with respect to the NLO result at  $\mu_F = \mu_R = m_Z$  (see Eq. (12)).*

at central value of the scales (central dot-dashed line) and the corresponding scale uncertainty (upper and lower dot-dashed lines). The NLO (solid lines) and LO (dashed lines) bands in Fig. 10 are exactly the same bands as those in Fig. 3. In the region where  $10 \text{ GeV} \lesssim q_T \lesssim 40 \text{ GeV}$ , the NLL+LO and NLO central values are quite close: their difference is, at most, of about 8%. Decreasing the value of  $q_T$ , the scale uncertainty at NLL+LO decreases from about  $\pm 20\%$  ( $q_T \sim 40 \text{ GeV}$ ), to about  $\pm 15\%$  ( $q_T \sim 20 \text{ GeV}$ ) and  $\pm 10\%$  ( $q_T \sim 10 \text{ GeV}$ ). We also recall our conclusions (see Sect. 3.1) about the uncertainty of the fixed-order perturbative expansion: the perturbative uncertainty of the NLO predictions is at the level of about  $\pm 20\%$  in the region where  $20 \text{ GeV} \lesssim q_T \lesssim 40 \text{ GeV}$  (see the upper line of the LO band), and it does not decrease at smaller values of  $q_T$ . We conclude that, at intermediate values of  $q_T$ , the NLL+LO and NLO results are fully consistent and have a comparable perturbative uncertainty. The NLL+LO calculation provides us with QCD predictions that can be extended to smaller values of  $q_T$  ( $q_T \lesssim 20 \text{ GeV}$ ) with a controllable and relatively-small perturbative uncertainty.

The bulk of the production cross section is contained in the small- $q_T$  region. Considering the region above the peak of the  $q_T$  distribution ( $2 \text{ GeV} \lesssim q_T \lesssim 20 \text{ GeV}$ ), the scale uncertainty of the NLL+LO calculation is below the level of about  $\pm 15\%$  (Fig. 9). The size of the scale uncertainty increases in the region below the peak. The effect of the scale variations is larger in the region below the peak since the shape of the  $q_T$  distribution is much steeper in this region (see Figs. 7 and 8). Note also that this region is expected to be most sensitive to NP effects. The sizeable

reduction of the scale uncertainty in the interval  $q_T \sim 3\text{--}7$  GeV can be accidental and, thus, it can underestimate the perturbative uncertainty of the NLL+LO result.

The detailed comparison in Fig. 9 shows that the experimental data are consistent with the NLL+LO predictions in the small- $q_T$  region. As in the case of Fig. 3, we also recall that part of the differences between data and theory have a systematic component due to the luminosity uncertainties and to the values of the total cross sections. In particular, the central value of  $d\sigma/dq_T$  at NLL+LO accuracy corresponds to the NLO values,  $\sigma = 226$  pb, of the total cross section; this value is about 9% smaller than the CDF value, and it is about 2% larger than the D0 value. These differences between the total cross sections are consistent with the fact that the NLL+LO result tends to agree better with the D0 data than with the CDF data.

The quantitative predictions presented up to now are obtained in a purely perturbative framework. It is known (see e.g. Ref. [13] and references therein) that the transverse-momentum distribution is affected by NP effects, which become important as  $q_T$  becomes small. A customary way of modelling these effects is to introduce an NP transverse-momentum smearing of the distribution. In the case of resummed calculations in impact parameter space, the NP smearing is implemented by multiplying the  $b$ -space perturbative form factor by an NP form factor. Different procedures to relate the two form factors and several different parametrizations of the NP form factor are available in the literature [39, 56, 23]; the corresponding NP parameters are obtained by global fits to DY data [23, 27, 57].

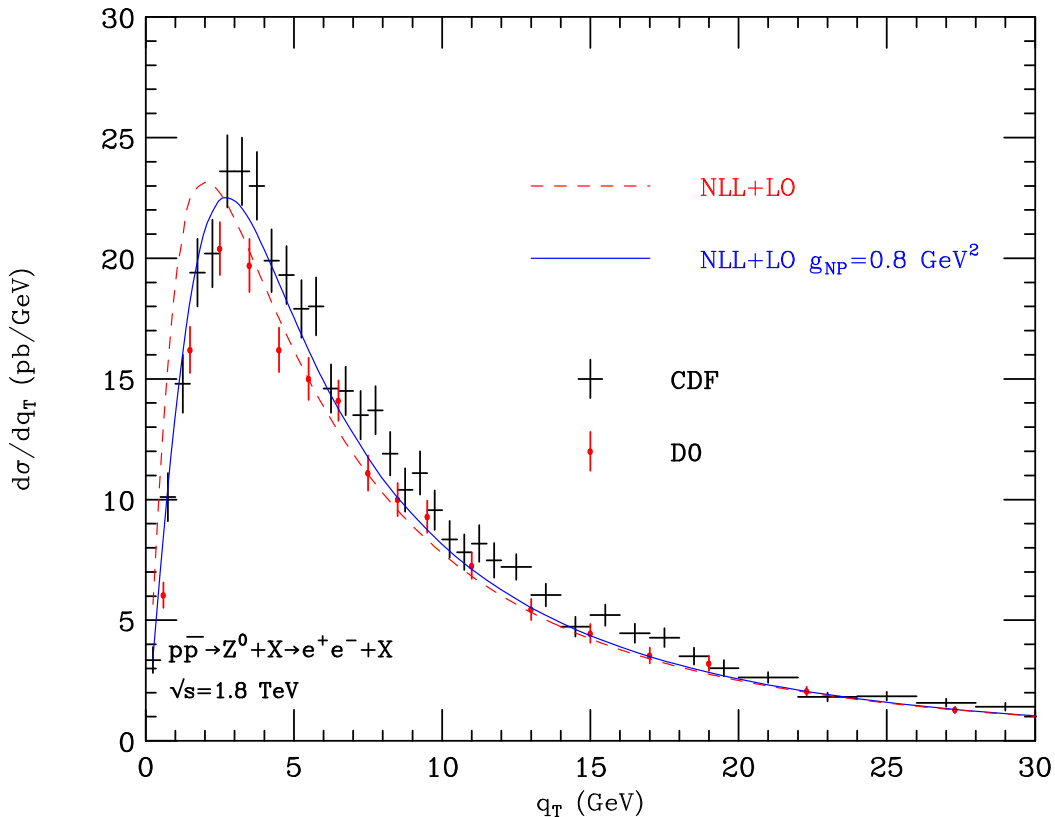


Figure 11: *The NLL+LO spectrum at the Tevatron Run I supplemented with the NP form factor of Eq. (15).*

A detailed study of the NP effects is beyond the aim of this work. We limit ourselves to illustrate the possible impact of NP effects on our resummed calculation. To this purpose, we simply multiply the  $b$ -space resummation factor  $\mathcal{W}_N^V(b, M)$  (see Eqs. (3) and (4)) by a NP factor,  $S_{NP}$ , which includes a gaussian smearing of the form

$$S_{NP} = \exp\{-g_{NP} b^2\}. \quad (15)$$

In Fig. 11 we show the NLL+LO distribution at central values of the scales with (solid) and without (dashed) the inclusion of the NP factor. The numerical value of the NP coefficient  $g_{NP}$  is taken to be  $g_{NP} = 0.8 \text{ GeV}^2$  [25]. Using this values of  $g_{NP}$ , the NP effects reduce (increase) the perturbative distribution where  $q_T \lesssim 3 \text{ GeV}$  ( $q_T \gtrsim 3 \text{ GeV}$ ). For instance, the NP correction is about  $-10\%$  at  $q_T \sim 2 \text{ GeV}$ , about  $+8\%$  at  $q_T \sim 5 \text{ GeV}$ , and it is smaller than  $+4\%$  where  $q_T \gtrsim 10 \text{ GeV}$ . As expected, the effect of the NP form factor is to make the distribution harder, thus improving the agreement with the experimental data at very small values of  $q_T$ . On the basis of the results in Ref. [29], we also expect that such NP effect is qualitatively similar to that produced by the inclusion of higher-order logarithmic contributions. This expectation is consistent with the fact that the quantitative impact of the NP form factor is within the perturbative uncertainty of the NLL+LO result (see Figs. 8 and 9). A detailed comparison of Tevatron data with a full NNLL+NLO calculation, including non-perturbative effects, is left to future work.

We have repeated our NLL+LO study by considering the normalized  $q_T$  distribution,  $\frac{1}{\sigma} \frac{d\sigma}{dq_T}$ , at the Tevatron Run II. The main features of the results are definitely very similar to those at Run I. The NLL+LO results at small and intermediate values of  $q_T$  are briefly summarized in Fig. 12. We show the NLL+LO distribution at central values of the scales with (solid) and without (dashed) the inclusion of the NP form factor (we use the same values of  $g_{NP}$  as in Fig. 11). Since the perturbative uncertainty is dominated by the effect of varying the resummation scale  $Q$ , we fix  $\mu_R = \mu_F = m_Z$  and we also show the NLL+LO results with  $Q = m_Z$  (dotdashed) and  $Q = m_Z/4$  (dotted). We observe that the D0 data are consistent with the NLL+LO predictions. We also observe that the experimental errors are smaller than the uncertainty of the NLL+LO results, thus demanding more accurate perturbative predictions.

## 4 Summary

We have considered the  $q_T$  cross section of DY  $e^+e^-$  pairs from the decay of  $Z$  bosons produced in  $p\bar{p}$  collisions at Tevatron energies.

We have presented fixed-order QCD predictions up to NLO, including an estimate of the corresponding perturbative uncertainty. In the region of large and intermediate values of  $q_T$ , the CDF and D0 data at Tevatron Run I show an overall agreement with the NLO results. Some deviations from the NLO predictions are observed in the Run II D0 data at moderate values of  $q_T$ . In the region of small values of  $q_T$ , the comparison between the LO and NLO results shows the onset of instabilities of the order-by-order perturbative expansion. As  $q_T$  decreases toward very small values, the fixed-order central values definitely disagree with the Tevatron data.

As is well known, in the small- $q_T$  region, there are large logarithmic contributions that spoil the reliability of the fixed-order perturbative expansion and that need be resummed to all orders. We have presented a first application of the resummation formalism of Refs. [29] to  $Z$  boson

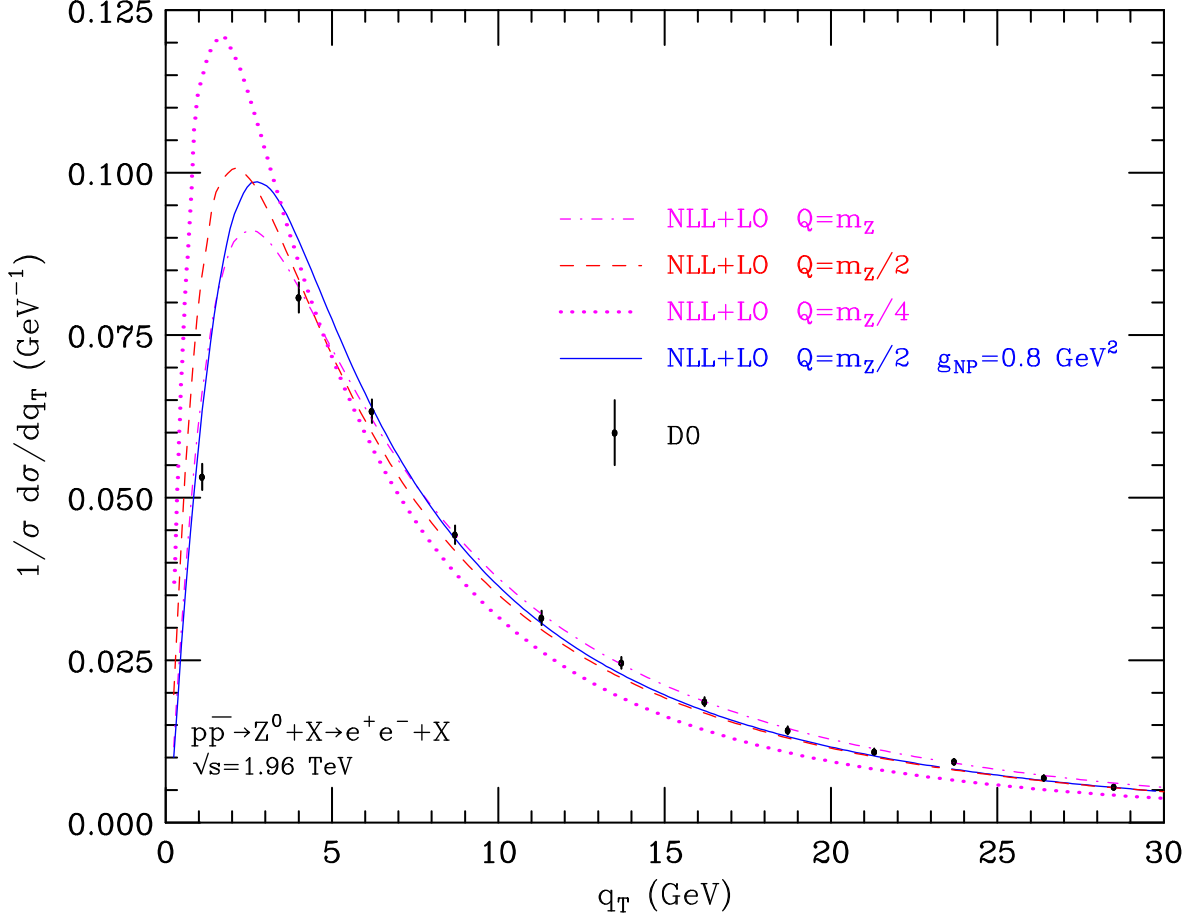


Figure 12: *The NLL+LO  $q_T$  spectrum at the Tevatron Run II, for different values of the resummation scale  $Q$ . The effect of including a NP smearing as in Eq. (15) is also shown.*

production. The formalism combines small- $q_T$  resummation at a given logarithmic accuracy with the fixed-order calculations. It implements a unitarity constraint that guarantees that the integral over  $q_T$  of the differential cross section coincides with the total cross section at the corresponding fixed-order accuracy. The formalism includes the explicit dependence on the factorization and renormalization scales, analogously to the customary scale dependence in fixed-order calculations. It also introduces an auxiliary resummation scale, whose dependence can be exploited to estimate the effect of uncalculated higher-order logarithmic contributions. Owing to these features, the resummation formalism extends the applicability of QCD perturbation theory to the small- $q_T$  region, with a controllable perturbative accuracy at small and intermediate values of  $q_T$ .

We have presented the results of the resummed calculation at NLL+LO accuracy, and we have performed a detailed study of the scale dependence to estimate the corresponding perturbative uncertainty. In the region of intermediate values of  $q_T$ , the NLL+LO and NLO results are fully consistent and have a comparable perturbative uncertainty. In the small- $q_T$  region, the Tevatron data are consistent with the NLL+LO predictions, which are not supplemented with additional non-perturbative contributions. The perturbative uncertainty of the NLL+LO results, which is dominated by missing higher-order logarithmic contributions, is relatively large in comparison with the precision of the experimental data. This uncertainty is likely to be comparable with

the effect of non-perturbative contributions. On the basis of the results on  $q_T$  spectrum of the Standard Model Higgs boson [30, 29, 31], we expect a reduction of the perturbative uncertainty once the complete NNLL+NLO calculation for the DY process is available.

## References

- [1] R. Hamberg, W. L. van Neerven and T. Matsuura, Nucl. Phys. B **359** (1991) 343 [Erratum-ibid. B **644** (2002) 403]; R. V. Harlander and W. B. Kilgore, Phys. Rev. Lett. **88** (2002) 201801.
- [2] C. Anastasiou, L. J. Dixon, K. Melnikov and F. Petriello, Phys. Rev. D **69** (2004) 094008.
- [3] K. Melnikov and F. Petriello, Phys. Rev. Lett. **96** (2006) 231803, Phys. Rev. D **74** (2006) 114017.
- [4] S. Dittmaier and M. Kramer, Phys. Rev. D **65** (2002) 073007; U. Baur and D. Wackerth, Phys. Rev. D **70** (2004) 073015; V. A. Zykunov, Phys. Atom. Nucl. **69** (2006) 1522 [Yad. Fiz. **69** (2006) 1557]; A. Arbuzov et al., Eur. Phys. J. C **46** (2006) 407 [Erratum-ibid. C **50** (2007) 505]; C. M. Carloni Calame, G. Montagna, O. Nicrosini and A. Vicini, JHEP **0612** (2006) 016.
- [5] U. Baur, O. Brein, W. Hollik, C. Schappacher and D. Wackerth, Phys. Rev. D **65** (2002) 033007; V. A. Zykunov, Phys. Rev. D **75** (2007) 073019; C. M. Carloni Calame, G. Montagna, O. Nicrosini and A. Vicini, JHEP **0710** (2007) 109; A. Arbuzov et al., Eur. Phys. J. C **54** (2008) 451.
- [6] R. K. Ellis, G. Martinelli and R. Petronzio, Nucl. Phys. B **211** (1983) 106.
- [7] P. B. Arnold and M. H. Reno, Nucl. Phys. B **319** (1989) 37 [Erratum-ibid. B **330** (1990) 284].
- [8] R. J. Gonsalves, J. Pawlowski and C. F. Wai, Phys. Rev. D **40** (1989) 2245.
- [9] Y. L. Dokshitzer, D. Diakonov and S. I. Troian, Phys. Lett. B **79** (1978) 269, Phys. Rep. **58** (1980) 269.
- [10] G. Parisi and R. Petronzio, Nucl. Phys. B **154** (1979) 427.
- [11] G. Curci, M. Greco and Y. Srivastava, Nucl. Phys. B **159** (1979) 451.
- [12] J. C. Collins and D. E. Soper, Nucl. Phys. B **193** (1981) 381 [Erratum-ibid. B **213** (1983) 545].
- [13] J. C. Collins and D. E. Soper, Nucl. Phys. B **197** (1982) 446.
- [14] J. Kodaira and L. Trentadue, Phys. Lett. B **112** (1982) 66, report SLAC-PUB-2934 (1982), Phys. Lett. B **123** (1983) 335.
- [15] G. Altarelli, R. K. Ellis, M. Greco and G. Martinelli, Nucl. Phys. B **246** (1984) 12.



- [16] J. C. Collins, D. E. Soper and G. Sterman, Nucl. Phys. B **250** (1985) 199.
- [17] S. Catani, D. de Florian and M. Grazzini, Nucl. Phys. B **596** (2001) 299.
- [18] P. B. Arnold and R. P. Kauffman, Nucl. Phys. B **349** (1991) 381.
- [19] C. Balazs, J. w. Qiu and C. P. Yuan, Phys. Lett. B **355** (1995) 548.
- [20] C. Balazs and C. P. Yuan, Phys. Rev. D **56** (1997) 5558.
- [21] R. K. Ellis, D. A. Ross and S. Veseli, Nucl. Phys. B **503** (1997) 309.
- [22] R. K. Ellis and S. Veseli, Nucl. Phys. B **511** (1998) 649.
- [23] J. w. Qiu and X. f. Zhang, Phys. Rev. Lett. **86** (2001) 2724, Phys. Rev. D **63** (2001) 114011.
- [24] A. Kulesza and W. J. Stirling, Eur. Phys. J. C **20** (2001) 349.
- [25] A. Kulesza, G. Sterman and W. Vogelsang, Phys. Rev. D **66** (2002) 014011.
- [26] E. L. Berger and J. w. Qiu, Phys. Rev. D **67** (2003) 034026, Phys. Rev. Lett. **91** (2003) 222003.
- [27] F. Landry, R. Brock, P. M. Nadolsky and C. P. Yuan, Phys. Rev. D **67** (2003) 073016.
- [28] S. Berge, P. M. Nadolsky and F. I. Olness, Phys. Rev. D **73** (2006) 013002.
- [29] G. Bozzi, S. Catani, D. de Florian and M. Grazzini, Nucl. Phys. B **737** (2006) 73.
- [30] G. Bozzi, S. Catani, D. de Florian and M. Grazzini, Phys. Lett. B **564** (2003) 65.
- [31] G. Bozzi, S. Catani, D. de Florian and M. Grazzini, Nucl. Phys. B **791** (2008) 1.
- [32] M. Grazzini, JHEP **0601** (2006) 095.
- [33] R. Frederix and M. Grazzini, Phys. Lett. B **662** (2008) 353.
- [34] G. Bozzi, B. Fuks and M. Klasen, Phys. Rev. D **74** (2006) 015001.
- [35] H. Kawamura, J. Kodaira, H. Shimizu and K. Tanaka, Prog. Theor. Phys. **115** (2006) 667; H. Kawamura, J. Kodaira and K. Tanaka, Nucl. Phys. B **777** (2007) 203, Prog. Theor. Phys. **118** (2007) 581, Phys. Lett. B **662** (2008) 139.
- [36] Y. Koike, J. Nagashima and W. Vogelsang, Nucl. Phys. B **744** (2006) 59.
- [37] S. Catani, E. D’Emilio and L. Trentadue, Phys. Lett. B **211** (1988) 335.
- [38] C. T. H. Davies and W. J. Stirling, Nucl. Phys. B **244** (1984) 337.
- [39] C. T. H. Davies, B. R. Webber and W. J. Stirling, Nucl. Phys. B **256** (1985) 413.
- [40] D. de Florian and M. Grazzini, Phys. Rev. Lett. **85** (2000) 4678, Nucl. Phys. B **616** (2001) 247.
- [41] S. Catani and M. Grazzini, Phys. Rev. Lett. **98** (2007) 222002, and preprint in preparation.

- [42] A. Vogt, Phys. Lett. B **497** (2001) 228; C. F. Berger, Phys. Rev. D **66** (2002) 116002.
- [43] S. Moch, J. A. M. Vermaseren and A. Vogt, Nucl. Phys. B **688** (2004) 101.
- [44] S. Frixione and B. R. Webber, JHEP **0206** (2002) 029; S. Frixione, P. Nason and B. R. Webber, JHEP **0308** (2003) 007.
- [45] S. Alioli, P. Nason, C. Oleari and E. Re, JHEP **0807** (2008) 060.
- [46] K. Hamilton, P. Richardson and J. Tully, JHEP **0810** (2008) 015.
- [47] E. Laenen, G. Sterman and W. Vogelsang, Phys. Rev. Lett. **84** (2000) 4296.
- [48] S. Catani, M. L. Mangano, P. Nason and L. Trentadue, Nucl. Phys. B **478** (1996) 273.
- [49] A. A. Affolder *et al.* [CDF Collaboration], Phys. Rev. Lett. **84** (2000) 845.
- [50] B. Abbott *et al.* [D0 Collaboration], Phys. Rev. Lett. **84** (2000) 2792, Phys. Rev. D **61** (2000) 032004.
- [51] V. M. Abazov *et al.* [D0 Collaboration], Phys. Rev. Lett. **100** (2008) 102002.
- [52] A. D. Martin, R. G. Roberts, W. J. Stirling and R. S. Thorne, Eur. Phys. J. C **28** (2003) 455.
- [53] A. D. Martin, R. G. Roberts, W. J. Stirling and R. S. Thorne, Phys. Lett. B **604** (2004) 61.
- [54] J. Campbell, R.K. Ellis, *MCFM - Monte Carlo for FeMtobarn processes*, <http://mcfm.fnal.gov>.
- [55] B. Abbott *et al.* [D0 Collaboration], Phys. Rev. D **61** (2000) 072001.
- [56] G. A. Ladinsky and C. P. Yuan, Phys. Rev. D **50** (1994) 4239; F. Landry, R. Brock, G. Ladinsky and C. P. Yuan, Phys. Rev. D **63** (2001) 013004; S. Berge, P. M. Nadolsky, F. Olness and C. P. Yuan, Phys. Rev. D **72** (2005) 033015.
- [57] A. Kulesza and W. J. Stirling, JHEP **0312** (2003) 056; A. V. Konychev and P. M. Nadolsky, Phys. Lett. B **633** (2006) 710.